Waves in ice

Luke G. Bennetts

University of Melbourne, Parkville, VIC 3010, Australia

Abstract

Ocean surface waves can propagate long distances through regions containing floating ice covers. The impacts ocean waves have on the ice covers are of interest in the climate change era, as the polar regions experience pressure from rising temperatures. This chapter provides a review of observations and theoretical models for ocean wave propagation through the marginal ice zone, landfast ice and ice shelves. It traces the historical evolution of the field, from seminal work in the 1970s80s up to recent research advances. Key research questions are identified for each of the three ice covers, and commonalities between them are highlighted. The chapter concludes with perspectives and outlooks on the field of waves in ice, in the context of the dramatic changes currently occurring to the world's sea ice and ice shelves.

- A synthesis of research on ocean wave propagation through landfast ice, ice shelves and the marginal ice zone
- Observations and theories reviewed for waves in each of the three types of ice-covered waters
- Key research questions identified and overlaps highlighted between the sub-fields
- Future research focus on the coupled marginal ice zone–landfast ice–ice shelf system is called for

Keywords: ocean waves; wave–ice interactions; landfast ice; marginal ice zone; ice shelves; field observations; theoretical models; wave attenuation; wave scattering; wave energy dissipation; viscoelasticity; ice shelf vibrations

1 Introduction

The phrase "waves in ice" has been broadly adopted as an abbreviation for "ocean wave propagation through ice-covered waters". It has become synonymous with studies of the marginal ice zone, which is the tens to hundreds of kilometres wide outer region of the sea ice-covered ocean, where surface waves from the open ocean regularly influence the ice cover by breaking up larger ice floes, preventing the ice cover from consolidating, and more [Bennetts et al., 2024a]. Marginal ice zone dynamics has resurfaced as an area of major international research activity since the early 2010s [Bennetts et al., 2022a]. The renewed activity was initially driven by retreat of Arctic sea ice and the associated shift of the Arctic sea ice cover towards more marginal ice zone-type conditions [Squire, 2011] but is now equally motivated by understanding the response of Antarctic sea ice to climate change. Substantial advances have been made, including dedicated experiments during field campaigns, including the second Sea Ice Physics and Ecosystems eXperiment (SIPEX II) in the eastern Southern Ocean in 2012 [Kohout et al., 2014], the SeaState campaign in the western Arctic Sea in 2015 [Thomson et al., 2018], and the Polynyas, Ice Production and seasonal Evolution in the Ross Sea (PIPERS) in 2017 [Kohout et al., 2020]. The research focus has been on understanding and modelling wave attenuation over distance due to the ice cover, with a sub-focus on how the ice cover affects the directional wave spectrum, as these inform predictions of the distribution of wave energy in the marginal ice zone, which is the basis for modelling wave impacts on the ice cover [Bennetts et al., 2022b]. The advances build on seminal work conducted in the 1970s–1980s, led by members of the University of Cambridge's Scott Polar Research Institute, which included large experimental programmes, such as the Arctic marginal ice zone experiments (MIZEX 1983, etc.) and the Labrador ice margin experiment (LIMEX), and theoretical modelling in the 1990s–2000s, primarily by New Zealand-based researchers [Squire, 2022a, Bennetts et al., 2022a]. However, key research questions remain about waves in the marginal ice zone, as well as other aspects of marginal ice zone dynamics [Squire, 2022b].

Waves in ice also encompasses ocean wave propagation through landfast ice, which is sea ice attached to the coast, and through ice shelves (and ice tongues), which are the extensions of grounded (freshwater) ice sheets onto the ocean surface that enclose sub-shelf water cavities. These two forms of floating ice occupy large proportions of the Antarctic coastline, and are also found around land masses in the Arctic Ocean. The key research questions for waves in these ice types overlap with those for waves in the marginal ice zone. They were topics of research activity in a similar era to the early research drive on waves in the marginal ice zone, and often led by the same research groups. They have become active research areas again over the past one to two decades, although not at the same level of research intensity as waves in the marginal ice zone.

For landfast ice, the aim is to understand and predict breakup of the ice cover due to ocean waves that reach coastal regions during lows or absence of surrounding pack ice [Crocker and Wadhams, 1989]. As such, there is a focus on wave attenuation over distance travelled through landfast ice. The topic has been revisited by researchers primarily interested in the marginal ice zone, who viewed it as providing a simplified version of the attenuation problem, because ocean waves propagate through landfast ice-covered waters as ice-coupled waves known as flexural-gravity waves, whereas their form is undetermined in the granular ice covers that occupy the marginal ice zone. There has also been a strong focus on refection of incident wave energy by the landfast ice edge and the resulting proportion of energy transmitted as flexural-gravity waves.

Ice shelves are tens to hundreds of metres thick at the shelf front, compared to decimetres to metres for sea ice, which means the ice shelf front (its seaward edge) reflects short waves, and only long ocean waves penetrate into the ice shelf. There is strong evidence that long waves over a broad spectrum, from long swell, to infragravity waves, to tsunamis, force ice shelf flexure that triggered major calving events [Brunt et al., 2011, Bromirski et al., 2010, Massom et al., 2018, Zhao et al., 2024]. As such, a key research question is on how waves interact with ice shelf fractures and other weaknesses. Large ice shelf thickness also means that multiple propagating wave modes are likely to exist, and assessing the regimes in which these modes are significant is a topic of current research interest.

There are existing review articles on or including waves in sea ice. The highly cited "of ocean waves and sea ice" trilogy [Squire et al., 1995, Squire, 2007, 2020] and one independent review article [Shen, 2019] cover waves in landfast ice and waves in the marginal ice zone. A theme issue of *Philosophical Transactions A* on marginal ice zone dynamics [Bennetts et al., 2022a] includes a collection of articles on waves in the marginal ice zone, spanning observations [Waseda et al., 2022], physical modelling [Toffoli et al., 2022], numerical modelling [Perrie et al., 2022], a review of wave dissipation theory [Shen, 2022], and a general overview [Thomson, 2022]. Concise reviews of waves in the marginal ice zone appear in broader review articles on modelling sea ice [Golden et al., 2020] and Southern Ocean dynamics [Bennetts et al., 2024b], and of waves in landfast ice in a review of that ice type [Fraser et al., 2023]. There is currently no review of research on waves in ice shelves.

In this chapter, we give a chronology of findings from field observations of waves in landfast ice, ice shelves and the marginal ice zone, from the contemporary perspective of the key research questions outlined above for each of the three ice types. We follow this with an introduction to theoretical waves-in-ice models, with an emphasis on the close connections between the theories between the different ice types. Thus, the chapter synthesises waves-in-ice knowledge derived from observations and the associated theories. Physical models of waves in ice and numerical models that incorporate waves-in-ice theories are not covered. Further, waves in ice due to local sources, such as those created by winds over the marginal ice zone, moving loads on landfast ice and icequakes in ice shelves, are considered out-of-scope. Within these confines, the literature covered for waves in landfast ice and ice shelves is intended to be near comprehensive, but the large corpus of literature on waves in the marginal ice zone has meant that the studies reviewed are chosen to best illustrate the themes of the chapter.

2 Field observations

2.1 Landfast ice

Observations of waves in landfast ice were once considered to be more challenging than those in the marginal ice zone, as early attempts failed due to rapid breakup of the ice before the instruments were deployed and fully functioning [Squire et al., 1995]. The first field experiment to claim limited success was conducted in Newfoundland during 1977, in which ice-coupled waves propagating through landfast ice were recorded by a set of closely spaced devices and used to calculate the dispersion relation [Squire and Allan, 1977]. A far more extensive set of field measurements were collected as an opportunistic side experiment during MIZEX 1983, on ≈ 1 m thick "mushy" landfast ice in the fjords of Svalbard, such that the ice was attached to land on all sides but at the ice edge [Squire, 1984a]. Two vertical accelerometers were deployed on the landfast ice cover, with one device ≈ 5 m from the ice edge and the second device farther from the ice edge, and moved between different locations up to 400 m from the first device and recording for 0.5 h on each deployment. Significant wave heights up to 0.1 m were measured, and cracks were observed to appear during the experiment up to ≈ 50 m from the ice edge, which were attributed to wave-induced ice flexure. The measurements showed ice-coupled wave energy attenuates by an order of magnitude or more over only a few hundred metres, such that short period wave components experience the strongest attenuation. The components of the wave energy (density) spectrum were shown to display local extrema within the first few tens of metres from the ice edge, followed by an approximately exponential rate of decay away from the ice edge. Exponential attenuation rates of wave energy, α, were found by fitting exponential curves to the data points, with values on the order of 10^{-3} per metre at wave periods 6.8–8.5 s and 10^{-2} at 5.8 s.

More recent field observations of wave propagation through landfast ice have been made in both the Arctic and Southern oceans. Similar to MIZEX 1983 [Squire, 1984a], one experiment was conducted in a fjord of Svalbard [Sutherland and Rabault, 2016]. The experiment was conducted continuously over three days during March 2015, using three triaxial accelerometers deployed on 0.5–0.6 m thick landfast ice. One device was deployed $\approx$ 100 m from the ice edge and the two remaining devices were deployed close to one another, around 50 m farther onto the ice cover. The dispersion relation was found to be gravity dominated for low frequencies (0.08–0.12 Hz or 8.3–12.5 s), transitioning to flexure dominated for higher frequencies, although the transition to high-frequency flexure dominance was lost after a day into the experiment, which was attributed to the appearance of cracks in the ice cover. Strong attenuation (up to 80% between the sensors) was found only for frequencies > 0.15 Hz (or < 6.3 s) and before cracks appeared in the ice cover. There was evidence of counter propagating waves at high frequencies, which were inferred as wave scattering, although the scattering source was unknown. A subsequent experiment was conducted in a nearby Svalbard fjord and analysed alongside an experiment conducted on landfast ice north of Casey station in Antarctica, where the ice cover is not confined by sidewalls in a relatively narrow channel, as in the Svalbard fjords [Voermans et al., 2021]. Two inertial motion units were deployed on the landfast ice to record waves in both experiments. The Arctic experiment lasted two weeks and the ice was 0.3–0.4 m thick, whereas the Antarctic experiment lasted three to four weeks during October 2020 and the ice was 1.1–1.3 m thick. The Arctic data showed attenuation rates, α, that decrease from order 10^{-3} per metre at wave periods approximately 6 s or below and then 10^{-4} per metre up to 15 s. The Antarctic data were found to be unreliable for determining attenuation, and the results were scattered, although with magnitudes order 10^{-4} per metre, i.e., comparable with those from the Arctic.

2.2 Marginal ice zone

The first recordings of waves in the marginal ice zone were made in 1959–1960 (before the term marginal ice zone had been coined) on outbound and return voyages through the Antarctic ice pack in the Weddell Sea using a ship-borne recorder [Robin, 1963]. The recordings were made for ten minutes every six hours and were accompanied by visual estimates of ice thickness, floe size and concentration. The observations were the basis for a seminal study [Robin, 1963], which identified many key processes that remain topics of research activity today, such as the relationship between wavelengths and floe lengths. It took until the early 1970s for further observations to be reported [Wadhams, 1975, 1978]. They were made in the Arctic, where the waves and ice were measured remotely by an airborne laser profiler [Wadhams, 1975] and an echo sonar on a submarine [Wadhams, 1978], which avoids contamination of the measurements by the ship. The accompanying studies were also seminal, as they introduced the paradigm that the frequency components of the wave energy spectrum attenuate exponentially with distance into the sea ice-covered ocean, and that the attenuation rate, α, has a power-law relationship with frequency, f, of the form

$$\alpha = c\, f^{n}. \tag{1}$$

The attenuation coefficients were found to be around order 10^{-4} per metre and the power-law exponent $n \approx 2$–2.7. They also highlighted the importance of concomitant observations of the ice cover properties, which they achieved using aerial photography and an infrared scanner [Wadhams, 1975] or inferred from the sonar and visual observations using a periscope [Wadhams, 1978]. Higher attenuation was observed for more densely packed floe fields, which was attributed to frictional dissipation between floes [Wadhams, 1978].

From 1978–1984, members of the Scott Polar Research Institute embarked on a series of experiments to measure wave evolution through Arctic marginal ice zones, using helicopters to move from floe to floe and deploying accelerometers on the floes. The deployments on each floe were typically limited to tens of minutes and the analyses relied on the assumption that the incident field was statistically stationary over the experiment, such that the observations from multiple floes could be compared. One experiment was conducted in the Bering Sea during spring 1979 in a marginal ice zone consisting of ≈ 0.5 m-thick, "mushy" ice floes, with a 5 km-wide, diffuse edge zone of ≈ 10 m-diameter floes, and an interior zone of large floes (diameters > 100 m) starting 30 km away from the ice edge, separated by a transition zone where the floe diameter steadily increased over distance up to 40 m [Squire and Moore, 1980]. Another experiment was conducted in the Greenland Sea during MIZEX 1984 [Wadhams, 1985], which consisted of four runs at different locations and on different dates, where the reported floes were relatively thick (2–3 m) and large (diameters 72–350 m) and at a range of concentrations [Wadhams et al., 1986]. The 1979 Bering Sea experiment [Squire and Moore, 1980] was revisited and compared against experiments in the Greenland Sea during September 1978, September 1979 and July 1983, and the Bering Sea during February 1983 [Wadhams et al., 1988]. The findings support the concept of exponential attenuation over distance of the wave energy spectral components, with the attenuation rate, α, of order 10^{-4}–10^{-5} per metre [Squire and Moore, 1980, Wadhams et al., 1986, 1988]. The attenuation rate was found to increase linearly with ice thickness [Wadhams et al., 1988]. Multi-axial devices were used during MIZEX 1984, such that the directional wave spectrum was retrieved [Wadhams et al., 1986]. The observations showed that high frequencies ("wind seas") broaden to become isotropic after < 5 km, whereas swell initially narrows before broadening and becomes isotropic after tens of kilometres [Wadhams et al., 1986]. The broadening was attributed to wave scattering by floes, which competes with increased attenuation of directional components of the spectrum due to longer path lengths travelled to reach an observation location within the marginal ice zone.

By the early 1990s, analysis techniques for synthetic aperture radar (SAR) images had advanced to the point at which they could be used to study wave propagation in the marginal ice zone [Wadhams and Holt, 1991, Liu et al., 1991a,b, Larouche and Cariou, 1992]. SAR snapshots of the wave field over multiple-kilometre scales were used, and were processed to obtain wavenumber spectra. Airborne SAR images obtained during LIMEX in March 1987 of compacted and rafted floes with < 20 m diameters in a brash ice matrix were combined with accelerometer and wave buoy measurements to compute the ice-coupled dispersion relation, as well as the attenuation rate of the peak spectral components [Liu et al., 1991a] and provide evidence of refraction at the ice edge in the form of a wave energy cut-off beyond a critical incidence angle (similar to that found for landfast ice) [Liu et al., 1991b]. A subset of the LIMEX SAR data was re-assessed using a parametric spectral-density estimation technique [Larouche and Cariou, 1992], and used, for instance, to calculate the exponential attenuation rate for the low-frequency spectral components (periods > 12 s), which were found to be around half those calculated using accelerometer data, although noting the open-water dispersion relation was assumed in the calculations, and to provide evidence of wave refraction within the marginal ice zone, associated with a change in wavelength, which was attributed to a sharp change in ice concentration. A mosaic of two satellite-borne SAR images of waves in pancake–frazil ice covers in the Chukchi Sea during October 1978 were used to derive the wavenumber spectra in subregions of the imagery [Wadhams and Holt, 1991]. The observed reduction in dominant wavelength with distance into the ice cover and slight refraction towards the normal with respect to the ice edge were compared with a theory (mass loading; § 3.2), and combined with the theory to estimate the ice thickness. More extensive studies of waves in frazil–pancake icefields were conducted following acquisition of additional SAR data, including two Arctic experiments (in April 1993 and March 1997) and one Antarctic experiment in July 1997 [Wadhams et al., 2002], and then a further Antarctic experiment in April 2000 [Wadhams et al., 2004]. The studies provided evidence of a decrease in wavelength in the ice cover and refraction towards the normal direction.

From around the year 2000, technological advances allowed in situ observations of waves in the marginal ice zone to be made over weeks to months, with the data tranmitted via satellites. An array of six buoys that each relayed (frequency) wave spectra every 3 h (calculated from ≈ 30 min timeseries of vertical accelerations), as well as the buoy locations, were deployed in the Weddell Sea marginal ice zone during advancing pancake–frazil ice condition in April 2000 [Doble and Bidlot, 2013, Doble et al., 2015]. Attenuation rates, α, were calculated using observations from pairs of buoys over a 12-day period that covered an ice compression phase and a following re-expansion phase. A linear increase in the attenuation rate with increasing ice thickness was found during the compression phase, using model outputs for ice thickness [Doble et al., 2015]. One of the buoys survived until October 2000, and its final two months of observations captured a large wave event that broke the ice cover, as inferred from satellite-derived ice concentrations, and showed a significant increase in wave energy reaching the buoy following the breakup event, indicating that waves propagate more easily through broken ice covers [Doble and Bidlot, 2013].

The wave buoy-array approach was extended during SIPEX II, for which five bespoke buoys were deployed on the surfaces of ice floes in the East Antarctic marginal ice zone in September 2012 (which also relayed frequency spectra based on ≈ 30 min timeseries every 3 h) [Kohout et al., 2014, Meylan et al., 2014]. The buoys provided concomitant observations of wave spectra at different distances into the marginal ice zone along a meridional transect, from 16 km to 130 km from the ice edge, for up to 39 days, although they lost their alignment as they drifted north-eastward. The relative measurements of pairs of buoys indicated that the significant wave height, H_s (a proxy for the integrated energy spectrum) attenuates at an exponential rate over distance for mild conditions ($H_s < 3$ m) and linearly for more energetic conditions ($H_s > 3$ m) [Kohout et al., 2014], and that the exponential attenuation rate of the spectral components is related to frequency, such that

$$\alpha \approx a\,f^2 + b\,f^4, \tag{2}$$

where $a = 2.12 \times 10^{-3}\,\mathrm{s^2\,m^{-1}}$ and $b = 4.59 \times 10^{-2}\,\mathrm{s^4\,m^{-1}}$ [Meylan et al., 2014].

Wave buoy arrays have been deployed in the marginal ice zone during two subsequent field campaigns. Six wave experiments were conducted in the Arctic marginal ice zone from October–November 2015 during the SeaState campaign, where the ice cover was dominated by pancake–frazil ice [Cheng et al., 2017, Collins et al., 2018, Montiel et al., 2018]. Each wave experiment lasted hours to days, using up to seventeen wave buoys of three different types, where the buoys were recovered and reused for the subsequent experiments. Directional wave spectra were estimated from the timeseries given by each buoy split into 30 min segments. The buoy-pair approach (adapted to include wave direction) showed attenuation rates, α, ranging over order 10^{-7}–10^{-2} per metre [Cheng et al., 2017]. A single experiment involving a large wave event (up to $H_s \approx 5$ m measured) was analysed in detail, with the major findings being support for the transition from exponential to linear attenuation of the significant wave height at $H_s \approx 3$ m, evidence of a similar (although less clearly defined) switch for the spectral components, and narrowing of the wave direction over distance [Montiel et al., 2018]. The same experiment was the focus of a study on wave dispersion, which found almost no deviation from open water dispersion for frequencies < 30 Hz and a slight increase in wavenumber relative to open water for higher frequencies [Collins et al., 2018].

An extended version of the SIPEX II waves-in-ice observations were made during the PIPERS campaign, in which fourteen wave buoys were deployed on floes along a meridional transect of the Ross Sea marginal ice zone in autumn 2017 [Kohout et al., 2020, Rogers et al., 2021, Montiel et al., 2022]. Each buoy relayed the frequency wave spectra based on 11 min timeseries, typically every 15 mins, and operated for up to three months, creating the largest database of wave buoy observations to date and capturing large wave events, including significant wave heights > 9 m [Kohout et al., 2020]. In contrast to previous studies [Kohout et al., 2014, Montiel et al., 2018], the significant wave height was found to attenuate exponentially, even for large waves, although with indications for increases in the attenuation rate at higher concentrations and shorter periods [Kohout et al., 2020]. The attenuation rates of the spectral components from the full dataset were investigated using the buoy-pair approach [Montiel et al., 2022], and from a 24-day subset of the data by optimising the exponential attenuation rates of the spectral components in the WAVEWATCH III model to match the observations [Rogers et al., 2021]. The studies support power-law relationships of either binomial form (2) [Rogers et al., 2021] or monomial form (1) with exponent $n = 3.5$–4 [Rogers et al., 2021] or $n \approx 3$ within a few tens of kilometres from the ice edge, decreasing to $n < 2$ over 100 km from the ice edge [Montiel et al., 2022]. Both studies correlated changes in the attenuation rates with co-located variables (or "physical drivers"), finding strong evidence that the attenuation rate increases with ice thickness and decrease with significant wave height [Rogers et al., 2021], and increases with opposing (southerly) winds [Montiel et al., 2022].

Some smaller scale buoy observations are also notable. A single buoy was deployed in the winter Antarctic marginal ice zone during a cyclone that captured a significant wave height > 6 m at over 100 km from the ice edge [Vichi et al., 2019, Alberello et al., 2020]. Another buoy captured observations for almost a year in the Antarctic ice pack, during which it detected a significant wave height ≈ 0.1 m over 1000 km from the ice edge [Nose et al., 2024]. Two drifting wave buoys operated in the western Antarctic marginal ice zone during winter 2018, with a third in the open ocean close to the ice edge observing the incident wave fields [Ardhuin et al., 2020]. The observations show wave fields at 200 km from the ice edge with heights up to 1 m and narrow directional distributions (spreads $< 20°$).

Over the past decade, in concert with the proliferation of in situ observations, there has been a resurgence in studies of waves in the marginal ice zone using remote sensing observations. A technique was developed for measuring directional wavenumber spectra in the marginal ice zone using airborne scanning LIDAR [Sutherland and Gascard, 2016, Sutherland et al., 2018], extending the previous single-point airborne laser profiling measurements [Wadhams, 1975]. The method was demonstrated for observations along a 60 km transect of the Arctic marginal ice zone, taken from a aircraft over a 17 min period in late April 2006, for a broken ice field in which the maximum floes sizes (captured from a camera on the aircraft) were ≈ 50 m (less than half the dominant wavelength) [Sutherland and Gascard, 2016]. The directional wave spectrum was calculated for each 4 km segment of the flight, and used to show wave energy attenuation over distance, with a concomitant increase in peak wavelength and broadening of the directional spectrum [Sutherland and Gascard, 2016]. Similar measurements were made from five aircraft flights during the SeaState campaign, and data from two of the flights were found to be usable for waves-in-ice analysis [Sutherland et al., 2018]. For one flight, where the incoming wave field was near orthogonal to the ice edge, attenuation rates, α, of order 10^{-4}–10^{-2} per metre were calculated at up to 4 km from the ice edge, which indicated a power-law frequency dependence (1) with $n \approx 7/4$.

Methods have been developed to estimate wave heights in the marginal ice zone from SAR imagery over transects hundreds of kilometres long, although limited to long waves (swell) and, thus, only applicable at sufficient distances from the ice edge for short-wave components (wind seas) to become negligible [Ardhuin et al., 2015, 2017, Stopa et al., 2018a,b]. They have been applied to SAR data from Sentinel-1 satellites, including a set of images timed to coincide with the SeaState campaign that captured the large wave event during the campaign ($H_s > 4$ m), for which waves were detected > 100 km from the ice edge [Stopa et al., 2018a]. These observations showed exponential attenuation rates of significant waves heights of order 10^{-5} per metre before a network of leads (visible in the SAR imagery), weakening to order 10^{-6} per metre after the leads, which was hypothesised to result from the leads separating broken ice covers (before) from larger floes (after) [Stopa et al., 2018a]. More generally, Sentinel-1 satellites have been imaging Antarctic sea ice year-round since 2014, and over two thousand $20 \times 20\,\mathrm{km}^2$ images with suitable wave and ice conditions were analysed to find significant wave height attenuation rates spanning three orders of magnitude, with a median of 3×10^{-5} per metre [Stopa et al., 2018b]. A method to derive the 2D wave spectrum from SAR observations has also been developed and applied to images of the marginal ice zones of Svalbard and Greenland during March–April, 2021 [Huang and Li, 2023]. Attenuation rates of the resulting significant wave heights were order 10^{-5} per metre across fourteen analysed transects that included new, young and first-year ice, and the peak wave periods were 10–14 s.

Laser altimeter measurements of vertical displacements of the ocean surface from the IceSat-2 satellite have been used to infer waves in the marginal ice zone [Horvat et al., 2020, Brouwer et al., 2022, Hell and Horvat, 2024]. IceSat-2 has been operating since October 2018 and providing “near instantaneous” (ground speeds $7\,\mathrm{km\,s^{-1}}$) snapshots along transects of the Earth surface, including long stretches (hundreds to thousands of kilometres) of the sea ice-covered oceans in both hemispheres [Brouwer et al., 2022]. They are inhibited by cloud cover, and the vertical displacements due to waves must be decoupled from those due to sea ice, such that only 10–15% of the transects are usable [Brouwer et al., 2022]. Wave attenuation has been identified from the displacements and used to define the marginal ice zone width [Horvat et al., 2020, Brouwer et al., 2022], and limited validation against wave buoy measurements has been attempted in terms of significant wave heights [Brouwer et al., 2022]. A method to extract the wavenumber–direction wave spectra from altimeter measurements has been proposed and applied to a set of IceSat-2 transects [Hell and Horvat, 2024].

2.3 Ice shelves

As part of the International Geophysical Year program, 1957–1958, gravimeters that detect elevation changes were deployed on the upper surfaces of the Ross and Ronne–Filchner ice shelves, which are the two largest Antarctic ice shelves [Thiel et al., 1960]. The stations closest to the shelf fronts (2–5 km away), where the shelves were > 200 m thick, recorded tidal signals overlaid by “high frequency” oscillations (15–50 s periods), which were presumed to be ocean waves travelling through the shelves. The high-frequency oscillations were greatly reduced at stations farther from the shelf fronts (10–15 km away). In February 1958, during a spell of extensive open water offshore from the Ross Ice Shelf, the high-frequency oscillations close to the shelf front became so large that they exceeded the threshold of the gravimeter. Ice shelf oscillations attributed to ocean waves were also measured by gravimeters on the Ross Ice Shelf during the 1970s [Williams and Robinson, 1981]. A particular experiment used concurrent measurements from three stations at the southern end of the shelf, where the ice is 300–600 m thick, which provided evidence that ocean waves in the ice shelf manifest as flexural waves with speeds 50–65 m s^{-1}, although neglecting possible dispersive effects. Evidence was also found that short period waves attenuate over distance, and of resonances around wave periods of 17 s and 45 s.

In contrast to the early observations made on giant ice shelves, strain gauges were deployed on the surface of the Erebus Ice Tongue in the 1980s, for which the floating part of the tongue is only ≈ 10 km long, 0.5–2 km wide, and from 50 m thick at its snout (the seaward tip) to 300 m at its grounding line [Robinson and Haskell, 1992, Squire et al., 1994]. The strain gauges provided measurements from November 1984 to November 1989, which missed a large calving event by only months [Robinson and Haskell, 1990]. Maximum strains of 3×10^{-7} were measured during a storm event [Robinson and Haskell, 1992]. Evidence was found of waves travelling along the ice tongue, from the snout to the grounding line, with celerity ≈ 70 m s^{-1} and wave period ≈ 50 s, and were attributed to infragravity waves, which were a recently discovered concept [Robinson and Haskell, 1992]. Analysis of strain measurements on the surrounding sea ice over a few days in November 1989 also showed a 50 s peak, and with greater energy density than on the ice tongue [Squire et al., 1994].

A single broadband seismic station, consisting of one vertical and two horizontal seismometers, was deployed on the Ross Ice Shelf from November 2004 to November 2006, close to an anticipated calving site known as the Nascent Iceberg Rift [MacAyeal et al., 2006, Cathles IV et al., 2009, Bromirski et al., 2010, Bromirski and Stephen, 2012]. The seismometers were powered by sunlight, such that they recorded for 340 days outside of winter over the two-year deployment. Relatively large-motion swell events (≈ 7–40 s periods) and infragravity wave events (50–250 s) that originated from northern hemisphere storms were detected in spectrograms as slanting bands (caused by dispersion in the arrival time of the wave groups) [MacAyeal et al., 2006, Cathles IV et al., 2009, Bromirski et al., 2010]. Swell created amplitudes up to 30 mm [Cathles IV et al., 2009] and infragravity waves up to approximately three times greater, which was attributed to amplification by shoaling being more significant for longer waves [Bromirski et al., 2010].

The Ross Ice Shelf observations were extended to a 34-station seismic array from November 2014 to November 2016, where the stations were arranged into two linear transects that were approximately parallel and orthogonal to the shelf front, and with a dense subarray at the intersection of the transects [Bromirski et al., 2015, 2017, Chen et al., 2018, 2019]. The stations were powered by a combination of solar panels and lithium batteries, so that they could operate throughout the year. During austral summer, ten to twenty large swell events per month (10–30 s wave periods) were detected, reaching vertical amplitudes up to 4 mm at the stations closest to the shelf front, but showing significant attenuation away from the shelf front [Chen et al., 2018]. The horizontal amplitudes were smaller than the vertical amplitudes but attenuated more weakly away from the shelf front [Chen et al., 2018]. A large infragravity wave event (dominant energy in the 50–300 s wave-period band) was detected in May 2015, where the vertical displacements towards the shelf front were up to almost 10 mm but attenuating to ≈ 1 mm at 350 km from the shelf front [Bromirski et al., 2017]. Towards the shelf front, infragravity waves create near continuous vertical displacement of ≈ 2 mm amplitude [Chen et al., 2019], presumed to be due to infragravity waves bound to swell, as opposed to free infragravity waves that leak away from distant coastlines to create the large events [Bromirski et al., 2015]. A tsunami event was also captured, with dominant energy in the very-long period regime (300–1000 s wave-period band), which created vertical amplitudes over 10 mm without appreciable attenuation away from the shelf front, and were amplified at the station above a seabed protrusion [Bromirski et al., 2017]. The vertical displacements from one of the stations nearest the shelf front was analysed alongside observations of incoming waves from a nearby hydrophone mounted to the seabed just north of the shelf front, which indicated vertical ice shelf displacements relative to ocean wave displacements increase with wave period from order 10^{-2} at 30 s to just below unity at 100 s, and are relatively insensitive to wave period above 100 s [Chen et al., 2019]. Beamforming was also used to generate dispersion curves from the coherent wave signals over the dense subarray, and gave evidence of flexural-gravity waves for wave periods < 50 s from both the vertical and horizontal motions, and much faster extensional Lamb waves for 10–50 s wave periods from the horizontal motions [Chen et al., 2018]. In contrast, flexural-gravity waves extended into the swell regime from observation by a five-station array on the Pine Island Glacier during 2012–2013, which was attributed to the stations being closer to the shelf front, such that the swell had not attenuated [Chen et al., 2018].

3 Theoretical models

3.1 Waves in landfast ice

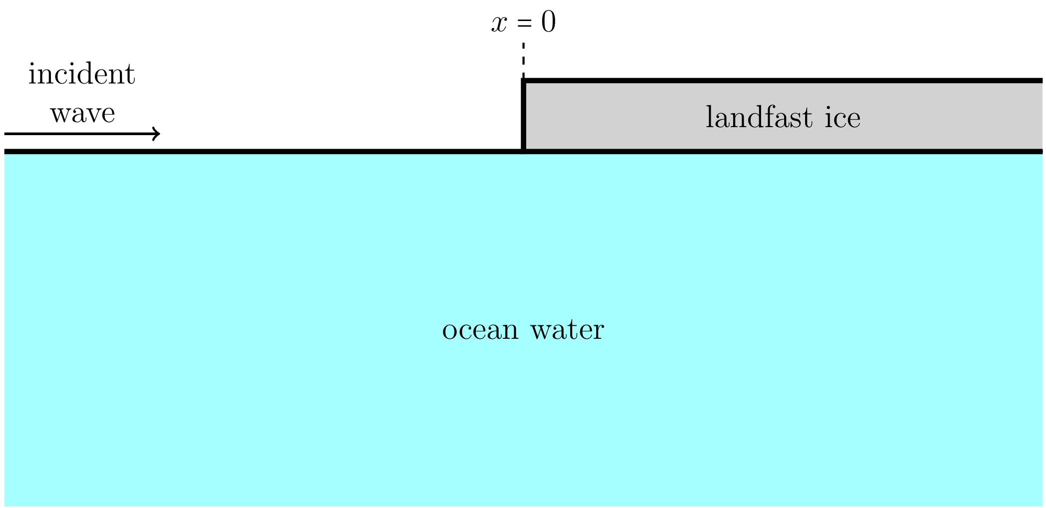

Figure 1: Schematic (not to scale) of the equilibrium geometry for the standard theoretical model of ocean wave interactions with landfast ice.

The standard theoretical model of ocean waves propagating into and through landfast ice treats the ice as a thin elastic Kirchhoff plate (or Euler–Bernoulli beam), floating on water that is modelled using potential-flow theory, i.e., the water is inviscid, incompressible and undergoes irrotational motions. Linear conditions are imposed, under the assumption that the amplitudes of motion are much smaller than the characteristic wavelengths, or, more simply, that the waves have small steepness. The canonical problem involves a water domain of infinite horizontal extent and ice of uniform properties and covering half of the water surface, so that the other half is open water, from which incident wave forcing is prescribed (Fig. 1). The water domain is typically assumed to be bounded below by a flat impermeable seabed at a finite depth, H [Fox and Squire, 1990, 1994, Chung and Fox, 2001].

Let t denote time, and the Cartesian coordinate system (x, y, z) denote locations in the water domain, where (x, y) denotes the horizontal location and z the vertical location. Without loss of generality, the ice edge is aligned along the y-axis ($x = 0$) and the origin of the vertical coordinate is located at the undisturbed water surface (Fig. 1). For convenience in solving the problem, it is common to assume the ice has no draught, so that its lower surface occupies the plane $z = 0$ for $x > 0$. Due to the thin-plate assumption, the flexural ice motion is determined solely from the vertical displacements of its lower surface, $\zeta(x, y, t)$ ($x > 0$). The function ζ extends to the open water region ($x < 0$) to denote the vertical displacements of the free surface. The water velocity field is defined as the gradient of a scalar function, $\Phi(x, y, z, t)$, known as a velocity potential, which satisfies Laplace's equation throughout the water domain.

It is convenient to map the problem from the time domain to the frequency domain (implicitly using a Fourier transform), and consider a time-harmonic problem at an arbitrary angular frequency, $\omega = 2\pi f$. Thus, the unknown surface displacement and velocity potential functions are, respectively,

$$\zeta(x, y, t) = \mathrm{Re}\{A_{\mathrm{inc}}\,\eta(x, y)\,\mathrm{e}^{-\mathrm{i}\omega t}\} \quad \text{and} \quad \Phi(x, y, z, t) = \mathrm{Re}\Big\{\frac{g\,A_{\mathrm{inc}}}{\mathrm{i}\,\omega}\phi(x, y, z)\,\mathrm{e}^{-\mathrm{i}\omega t}\Big\}, \tag{3}$$

where A_{inc} is the incident wave amplitude, $\mathrm{i} = \sqrt{-1}$ is the imaginary unit, $g = 9.81\,\mathrm{m\,s^{-2}}$ is the constant of gravitational acceleration, and η and ϕ are complex-valued functions. In the ice-covered region ($x > 0$), they are coupled at their common interface by the conditions

$$F\,\nabla_{\perp}^{4}\eta - \omega^2\,m\,\eta = \rho_w\,g\{\phi - \eta\} \quad \text{and} \quad \frac{\partial\phi}{\partial z} = \frac{\omega^2}{g}\eta \qquad (z = 0), \tag{4a,b}$$

where $\nabla_{\perp} \equiv (\partial/\partial x, \partial/\partial y)$, F is the flexural rigidity of the ice, m is its mass per unit area, and ρ_w is the water denity. Eq. (4a) is a dynamic condition that equates pressure exerted by the ice from thin-plate theory (on the left-hand side) with the water pressure from linearised Bernoulli theory (on the right). Eq. (4b) is a kinematic condition that sets the vertical velocity of the particles at the water surface (left-hand side) to be equal to the vertical velocity of the water surface. The coupling conditions assume the lower surface of the ice and the surface of the water below are in contact at all points such that $x > 0$, and at all times during the motion. Free-edge conditions are also applied to the ice edge, such that

$$\frac{\partial^2\eta}{\partial x^2} + \nu\,\frac{\partial^2\eta}{\partial y^2} = 0 \quad \text{and} \quad \frac{\partial}{\partial x}\left\{\frac{\partial^2\eta}{\partial x^2} + (2 - \nu)\,\frac{\partial^2\eta}{\partial y^2}\right\} = 0 \quad (x = 0), \tag{5}$$

where ν is Poisson's ratio, which represent vanishing of bending moment and shear stress, respectively. In the open water region ($x < 0$), the coupling conditions are

$$\eta = \phi \quad \text{and} \quad \frac{\partial\phi}{\partial z} = \frac{\omega^2}{g}\eta \quad (z = 0), \tag{6a,b}$$

where the dynamic condition (6a) is a degenerate version of (4a), and the kinematic condition (6b) is unchanged from (4b).

The ice displacement can be eliminated from the coupling conditions (4a–b) and (6a–b) to leave

$$F\,\nabla_{\perp}^{4}\frac{\partial\phi}{\partial z} - \omega^2\,m\,\frac{\partial\phi}{\partial z} = \rho_w\,g\left\{\frac{\omega^2}{g}\,\phi - \frac{\partial\phi}{\partial z}\right\} \qquad (x>0, z=0), \tag{7a}$$

$$\text{and}\quad \frac{\partial\phi}{\partial z} = \frac{\omega^2}{g}\,\phi \qquad (x<0, z=0). \tag{7b}$$

The free-edge conditions (5a–b) can also be expressed in terms of the velocity potential, as

$$\frac{\partial^2}{\partial x^2}\frac{\partial\phi}{\partial z} + \nu\,\frac{\partial^2}{\partial y^2}\frac{\partial\phi}{\partial z} = 0 \quad\text{and}\quad \frac{\partial}{\partial x}\left\{\frac{\partial^2}{\partial x^2}\frac{\partial\phi}{\partial z} + (2-\nu)\,\frac{\partial^2}{\partial y^2}\frac{\partial\phi}{\partial z}\right\} = 0 \quad (x=0, z=0). \tag{8}$$

These act as boundary conditions for Laplace's equation on the linearised water domain,

$$\nabla^2\phi = 0 \quad (x, y \in \mathbb{R}, -H<z<0), \quad\text{where}\quad \nabla \equiv (\partial/\partial x, \partial/\partial y, \partial/\partial z). \tag{9}$$

The seabed condition is

$$\frac{\partial\phi}{\partial z} = 0 \quad (z=-H), \tag{10}$$

which enforces no normal flow, assuming the seabed is impermeable.

Seeking separation solutions, $\phi(x,y,z) = X(x,y)\,Z(z)$, leads to the vertical modes

$$Z(z) = \cosh\{k\,(z+h)\} \quad\text{in the open water } (x<0), \tag{11a}$$

$$\text{and}\quad Z(z) = \cosh\{\kappa\,(z+h)\} \quad\text{in the ice-covered water } (x>0), \tag{11b}$$

with associated horizontal modes

$$X(x,y) = \mathrm{e}^{\pm\mathrm{i}\,(k_x\,x + k_y\,y)} \quad (x<0) \quad\text{and}\quad X(x,y) = \mathrm{e}^{\pm\mathrm{i}\,(\kappa_x\,x + \kappa_y\,y)} \quad (x>0), \tag{12a,b}$$

such that the wavevectors $\mathbf{k} = (k_x, k_y)$ and $\boldsymbol{\kappa} = (\kappa_x, \kappa_y)$ have magnitudes $|\mathbf{k}| = k$ and $|\boldsymbol{\kappa}| = \kappa$. The wavenumbers k and κ are the roots of dispersion relations, respectively,

$$k\,g\,\tanh(k\,H) = \omega^2 \quad\text{and}\quad \{F\,\kappa^4 + \rho_w\,g - m\,\omega^2\}\,\kappa\,\tanh(\kappa\,H) = \rho_w\,\omega^2. \tag{13a,b}$$

Eq. (13a) is the classical open water dispersion relation [Linton and McIver, 2001]. It has roots $k = \pm k_0, \pm k_1, \ldots$, where $k_0 \in \mathbb{R}_+$ supports propagating surface gravity waves, and $k_n \in \mathrm{i}\mathbb{R}_+$ $(n = 1, 2, \ldots)$, ordered such that $|k_1| < |k_2| < \ldots$, support so-called evanescent wave modes that decay exponentially away from scattering sources, such as an ice edge.

Eq. (13b) is the dispersion relation for a thin floating elastic plate, which has roots $\kappa = \pm\kappa_{-2}, \pm\kappa_{-1}, \pm\kappa_0, \pm\kappa_1, \ldots$. Similar to the open water dispersion relation, $\kappa_0 \in \mathbb{R}_+$, which supports propagating ice-coupled waves known as flexural-gravity waves, and $\kappa_n \in \mathrm{i}\mathbb{R}_+$ $(n = 1, 2, \ldots)$, such that $|\kappa_1| < |\kappa_2| < \ldots$, support evanescent wave modes. Flexural-gravity waves are shorter than gravity waves for short periods (i.e., $\kappa_0 > k_0$), for which mass loading dominates, and longer for long periods $(\kappa_0 > k_0)$ for which ice flexure dominates [Squire and Allan, 1977, Voermans et al., 2021], although certain observations suggest the effect of the ice cover becomes negligible when cracks appear in the ice [Sutherland and Rabault, 2016]. The wavenumbers κ_{-j} $(j = 1, 2)$ have no analogue in open water. They are typically complex valued, such that κ_{-1} is in the first quadrant of the complex plane and $\kappa_{-2} = -\overline{\kappa_{-1}}$, for which they support so-called damped-propagating waves [Squire et al., 1995]. However, they can also appear on the imaginary axis (similar to evanescent wavenumbers), and in these situations κ_{-1} and κ_{-2} no longer maintain their skew-conjugate relationship [Williams, 2006, Bennetts, 2007].

Let the incident wave from the open ocean, ϕ_{inc}, be propagating towards the ice cover (in the positive x-direction) at an angle $\psi \in [0, \pi/2)$ to the positive x-axis, so that

$$\phi_{\mathrm{inc}} = \mathrm{e}^{\mathrm{i}\, k_0\, \{\cos(\phi)\, x + \sin(\psi)\, y\}} \frac{\cosh\{k_0\,(z+H)\}}{\cosh(k_0\, H)}. \tag{14}$$

Uniformity of the geometry in the y-direction implies that the y-dependence of the incident wave can be enforced on the full solution, so that

$$\phi(x, y, z) = \varphi(x, z)\, \mathrm{e}^{\mathrm{i}\, k_0\, \sin(\psi)\, y}. \tag{15}$$

Applying this restriction to the y-components of the wavevectors $\mathbf{k}$ and $\boldsymbol{\kappa}$, i.e., $k_y = \kappa_y = k_0 \cos(\psi)$, means the x-components are

$$k_{x,n}^2 = k_n^2 - k_0^2 \cos^2(\psi) \quad (n = 0, 1, \ldots) \quad \text{and} \quad \kappa_{x,n}^2 = \kappa_n^2 - k_0^2 \cos^2(\psi) \quad (n = -2, -1, 0, 1, \ldots). \tag{16a,b}$$

Eq. (16b) results in two generic cases, with one case when $\kappa_0 \geq k_0$, for which $\kappa_x \in \mathbb{R}_+$ for all incident angles, so that a propagating wave exists in the ice-covered region, and the case where $\kappa_0 < k_0$, for which there is a critical angle $\psi_{\mathrm{crit}} = \arccos(\kappa_0 / k_0)$ that divides existence of a propagating wave mode ($\kappa_x \in \mathbb{R}_+$) for $\psi < \psi_{\mathrm{crit}}$ from decaying modes only ($\kappa_x \in \mathrm{i}\,\mathbb{R}_+$) for $\psi > \psi_{\mathrm{crit}}$.

The velocity potential, φ, is expressed as a linear superposition of wave modes defined by the dispersion relation in the relevant region (open or ice-covered water). In the open water region ($x < 0$), the wave field is the sum of the incident wave field, a leftward propagating reflected wave (amplitude $r_0^{(\mathrm{la})}$) and an infinite sum of evanescent waves that decay away from the ice edge (amplitudes $r_n^{(\mathrm{la})}$ for $n = 1, 2, \ldots$), so that

$$\varphi(x, z) = \mathrm{e}^{\mathrm{i}\, k_{x,0}\, x} \frac{\cosh\{k_0\,(z+H)\}}{\cosh(k_0\, H)} + \sum_{n=0}^{\infty} r_n^{(\mathrm{la})}\, \mathrm{e}^{-\mathrm{i}\, k_{x,n}\, x} \frac{\cosh\{k_n\,(z+H)\}}{\cosh(k_n\, H)} \quad (x < 0). \tag{17}$$

In the ice-covered region ($x > 0$), the wave field is a sum of a rightward propagating flexural-gravity wave (below the critical angle; amplitude $\tau_0^{(\mathrm{la})}$), the damped propagating waves (amplitudes $\tau_{-n}^{(\mathrm{la})}$ for $n = 1, 2$) and an infinite number of evanescent waves (amplitudes $\tau_n^{(\mathrm{la})}$ for $n = 1, 2, \ldots$ below the critical angle and $n = 0, 1, \ldots$ above it) that decay away from the ice edge, so that

$$\varphi(x, z) = \sum_{n=-2}^{\infty} \tau_n^{(\mathrm{la})}\, \mathrm{e}^{\mathrm{i}\, \kappa_{x,n}\, x} \frac{\cosh\{\kappa_n\,(z+H)\}}{\cosh(\kappa_n\, H)} \quad (x > 0). \tag{18}$$

The amplitudes associated with the two damped-propagating modes can be viewed as providing the degrees of freedom to satisfy the free-edge conditions (8a–b). The amplitudes of the propagating and evanescent wave modes in (17–18) then give the freedom to enforce continuity of pressure and horizontal velocity in the water column below the ice edge ($x = 0$, $-H < z < 0$).

For normal incidence ($\psi = 0$), activation of all the wave modes ($n = -2, -1, 0, 1, \ldots$) results in the only non-zero component of the ice strain (normal to the ice edge) increasing from zero at the ice edge to a constant amplitude once the damped-propagating and evanescent wave modes have died out away from the ice edge, with a maximum strain occurring inbetween for shorter wave periods [Fox and Squire, 1994]. The behaviour is less simple for non-normal incidence and below the critical angle, noting that the strain tensor has more than one non-zero component in this case [Fox and Squire, 1994]. For incidence at the critical angle and above it, the wave field can be expressed as a wave that travels parallel to the ice edge and decays away from it [Squire, 1984b].

The model outlined above does not produce the observed attenuation of waves through the landfast-ice-covered ocean [Squire, 1984a, Sutherland and Rabault, 2016, Voermans et al., 2021]. The standard model can be modified to include viscoelastic damping by using a complex-valued flexural rigidity, which was found to give reasonable agreement with observations of relatively large attenuation rates for near-melting landfast ice [Squire, 1984a]. An alternative modification incorporates damping using a term proportional to the ice displacement velocity [Robinson and Palmer, 1990], resulting in the dispersion relation

$$\{F\,\kappa^4 + \rho_w\,g - m\,\omega^2 - \mathrm{i}\,\omega\,\gamma\}\,\kappa\,\tanh(\kappa\,H) = \rho_w\,\omega^2, \tag{19}$$

where the damping parameter $\gamma = 10\,\mathrm{kPa\,m^{-1}}$ was found to predict attenuation in good agreement with one set of observations [Squire and Fox, 1992, Squire, 1993]. A range of wave damping models, broadly divided into those in which the damping occurs in the ice layer and those in which it occurs in the underlying water (in general, models not originally proposed for landfast ice), were compared against observations, with support for viscoelastic damping at shorter periods, and damping due to under ice turbulence and friction for longer periods [Voermans et al., 2021].

3.2 Waves in the marginal ice zone

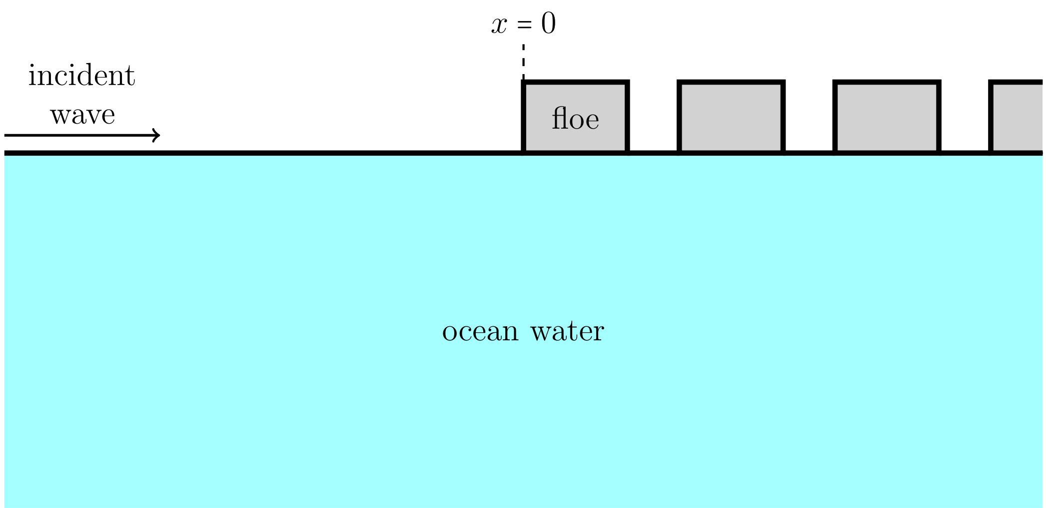

Figure 2: Schematic (not to scale) of the equilibrium geometry for a standard theoretical model of ocean wave propagation through the marginal ice zone.

In the classical model of waves in the marginal ice zone, the ice cover is treated as an array of floes separated by open water. The two-dimensional version of the model appears similar to the standard model for waves in landfast ice, except that the ice-covered region ($x > 0$) consists of multiple elastic plates of finite length (Fig. 2). Exponential wave attenuation over distance results, without damping, from an accumulation of scattering events by the individual floes, in which energy is reflected back towards the open ocean rather than being dissipated.

Consider the individual-floe version of the model, where the floe occupies the interval $x \in (0, \ell)$. On the left-hand side of the floe, the wave field is the sum of incident and reflected waves, plus evanescent waves generated at the floe edge, such that

$$\varphi(x, z) = \mathrm{e}^{\mathrm{i}\, k_{x,0}\, x} \, \frac{\cosh\{k_0\,(z + H)\}}{\cosh(k_0\, H)} + \sum_{n=0}^{\infty} r_n^{(\mathrm{fl})}\, \mathrm{e}^{-\mathrm{i}\, k_{x,n}\, x} \, \frac{\cosh\{k_n\,(z + H)\}}{\cosh(k_n\, H)} \quad (x < 0), \tag{20}$$

which is identical in form to Eq. (17). On its right-hand side, the wave field is a transmitted wave plus evanescent waves, such that

$$\varphi(x, z) = \sum_{n=0}^{\infty} t_n^{(\mathrm{fl})}\, \mathrm{e}^{\mathrm{i}\, k_{x,n}\, x} \, \frac{\cosh\{k_n\,(z + H)\}}{\cosh(k_n\, H)} \quad (x > \ell). \tag{21}$$

Thus $T^{(\mathrm{fl})} \equiv |t_0^{(\mathrm{fl})}|^2$ represents the proportion of the incident wave energy transmitted by the floe, and if the energy reflected by each floe is neglected, the wave energy transmitted by N identical floes is simply $(T^{(\mathrm{fl})})^N$. The is known as the single-scattering approximation, and results in the exponential attenuation rate

$$\alpha = -c \log\left(T^{(\mathrm{fl})}\right) / \ell \approx -c\, R^{(\mathrm{fl})} / \ell, \tag{22}$$

where c is the concentration of floes and $R^{(\mathrm{fl})} \equiv |r_0^{(\mathrm{fl})}|^2 = 1 - T$ (by energy conservation) is the proportion of wave energy reflected by an individual floe [Wadhams et al., 1988].

In general, the reflected energy increases with increasing frequency, so that the attenuation rate increases with frequency, consistent with observations. However, the reflection coefficient experiences sharp dips at certain resonant frequencies [Meylan and Squire, 1994], which cause corresponding dips in the attenuation rate that do not correspond to observations. This feature of the model can be alleviated by extending to a distribution of floe lengths and thicknesses, which is incorporated in the expression for the attenuation rate (22) in a straightforward manner [Wadhams, 1975]. Moreover, the expression for the predicted attenuation rate has been extended to include double scattering, which reduces the attenuation rate given by the single-scattering approximation by a factor $\approx 2/3$ [Wadhams et al., 1988]. These approximations, coupled with approximations of reflection by an individual floe, $R^{(\mathrm{fl})}$, were compared with many of the early observations by the Scott Polar Research Institute, and found, in general, to give reasonable agreement for mid-range wave periods, where the wavelengths are comparable to the floe sizes, which is the regime in which wave scattering is expected to dominate attenuation. For short periods the model predictions generally overpredict the observed attenuation rates and for long periods they underpredict the observations [Wadhams, 1975, 1978, Wadhams et al., 1988].

The full solution to the problem includes all orders of multiple scattering (reflections, re-reflections, re-re-reflections, etc.). The resulting wave field depends on the particular realisation of the ice cover, and, hence, so does the attenuation rate. For example, suppose the floes are identical and distributed according to some average concentration. In the case that the floes are equally spaced (a delta-function distribution), the waves that penetrate into the marginal ice zone (beyond $x > 0$) switch between frequency bands in which they propagate without attenuation and attenuate exponentially, which is the so-called passband/stopgap phenomenon known from other branches of wave science, but is not representative of waves observed in the marginal ice zone. If the locations of the floes are randomised strongly enough (assuming the concentration allows this freedom), then waves attenuate for all frequencies, due to the Anderson localisation phenomenon [Bennetts and Squire, 2012a]. For a given probability distribution, a single attenuation rate is derived by averaging over a large ensemble of solutions for randomly generated realisations of the ice cover [Kohout and Meylan, 2008, Bennetts and Squire, 2012a], where the averaging is with respect to wave energy rather than displacements, to avoid spurious additional attenuation due phase cancellations. If the randomisation is such that the waves transmitted by each floe are equally likely to have any phase, then the average attenuation rate over the ensemble can be found analytically to be $\alpha = -c \log(T^{(\mathrm{fl})}) / \ell$ [Bennetts and Squire, 2012a], i.e., the attenuation rate is identical to the single-scattering approximation (22). If the floes are long enough that interactions can be neglected between evanescent and decaying oscillatory waves generated at either floe end, and the floes are randomised, such that the flexural-gravity waves are equally likely to have any phase, then the expression for the attenuation rate can be reduced to

$$\alpha = -2\, c \log\left(1 - R^{(\mathrm{la})}\right) / \ell, \tag{23}$$

where $R^{(\mathrm{la})} \equiv |r^{(\mathrm{la})}|^2$ is the proportion of incident wave energy reflected in the landfast ice problem (§ 3.1) [Bennetts and Squire, 2012a]. Attenuation rate predictions from the full solution and approximation (23) have been compared with early observations, and, similar to the single- and double-scattering approximations, generally found to give reasonable agreement in the scattering regime but to overpredict and underpredict attenuation rates for short and long wave periods, respectively [Kohout and Meylan, 2008, Bennetts and Squire, 2012b].

Three-dimensional versions of the model have been developed, in which floes scatter waves in all directions across the ocean surface, in contrast to the two-dimensional model, which is restricted to backscattering only [Bennetts and Squire, 2009, Peter and Meylan, 2010, Bennetts et al., 2010, Montiel et al., 2016]. Studies using three-dimensional models predominantly use circular floes of uniform thickness for numerical efficiency [Peter et al., 2004], although, in principle, floes of arbitrary shape or non-uniform thickness could be studied [Meylan, 2002, Bennetts and Williams, 2010]. In one class of three-dimensional model, the floes are grouped into infinite periodic rows (lines of identical and equally spaced floes), where each row shares the same periodicity [Bennetts and Squire, 2009, Peter and Meylan, 2010, Bennetts et al., 2010]. The periodicity restricts the propagating component of the wave fields scattered by each row to a small set of plane waves [Bennetts and Squire, 2010], so that interactions between rows can be calculated efficiently [Bennetts and Squire, 2009, Peter and Meylan, 2010]. Attenuation rates predicted by this model were found to give good agreement with 1979 Bering Sea observations for wave periods from ≈ 6–9 s and reasonable agreement with 1979 Greenland Sea observations from 8–14 s [Bennetts et al., 2010]. Another class of three-dimensional model uses finite arrays, with no constraints on the ice floe arrangement. Innovative computational methods are required to simulate a large enough number of floes to represent a marginal ice zone, although boundary effects still plague analysis of the outputs [Montiel et al., 2016]. Model predictions of attenuation rates were found to underpredict observations in the Greenland Sea during the 1980s across the 5–15 s wave period range but to predict observed directional spreading of the wave field up to a 10 s period [Squire and Montiel, 2016].

The Boltzmann equation has been used an alternative theory to extend from the single-floe model to a model of the wave attenuation through marginal ice zone [Masson and LeBlond, 1989, Meylan et al., 1997, Meylan and Masson, 2006, Meylan and Bennetts, 2018]. The time-harmonic version of the resulting equation is of the form

$$(\cos\theta, \sin\theta)\cdot\nabla_{\perp}S = -q\,S + \frac{c}{A_{\mathrm{f}}}\int_{-\pi}^{\pi} K(\theta,\vartheta)\,S(x,y,\vartheta)\,\mathrm{d}\vartheta \quad \text{where} \quad q = \frac{c}{A_{\mathrm{f}}}\int_{-\pi}^{\pi} K(0,\vartheta)\,\mathrm{d}\vartheta, \tag{24}$$

A_{f} is the floe area, S is the wave energy density at location (x, y) in direction θ, and K is the scattering kernel derived from the single-floe model [Meylan et al., 1997, Bennetts and Williams, 2015]. It is referred to as a "phase-averaged" model, in contrast to the "phase-resolving" multiple-scattering models. Ensemble averaging with respect to configurations is implicit in the phase averaged property of the Boltzmann model. Moreover, the form of (24) fits naturally into the wave energy transport equations used in most numerical ocean wave models. (It has also been suggested that it can be approximated by an even simpler diffusion equation [Zhao and Shen, 2016].) However, over long distances, the Bolzmann equations predicts a steady wave field of finite energy [Meylan et al., 1997], which contrasts with exponential attenuation over distance predicted by phase-resolving models.

When the incident wavelengths are much greater than the floe sizes, the waves "see" the floes as a homogenised layer on the ocean surface, rather than a collection of individual floes, and, thus, the theoretical model becomes deterministic. In this regime, wave attenuation is dominated by dissipation of energy during wave–floe interactions, although the dominant dissipative mechanism(s) are debated. The attenuation rate for the homogenised medium can be calculated from the classical problem (Fig. 2) with some form of dissipation included (e.g., using Eq. 19), in the limit that the ratio of the floe size to the wavelength tends to zero [Pitt and Bennetts, 2024]. The attenuation rate tends to increase as the ratio decreases, although the effect of the ice edge on the incident waves decrease, which is also indicated by physical models [Dolatshah et al., 2018, Passerotti et al., 2022] and provides an explanation of the observations of increased wave activity after a breakup events.

It is more common to postulate the form of the homogenised medium with one or more free parameters (usually associated to the rate of dissipation) [Shen, 2022]. This approach is likely to capture waves-in-ice physics that would not in appear in the small-floe limit of the classical model. Calculation of the attenuation rate reduces to solving a dispersion relation to find a "dominant" wavenumber, which is usually the propagating wavenumber that has been perturbed into the complex plane by the dissipation [Meylan et al., 2018]. The attenuation rate of wave energy over distance is $\alpha = -2\,\mathrm{Im}\{\kappa_0\}$, where the free parameters are usually tuned such that the attenuation rate gives a best fit to observations.

Seminal models that treat the ice layer as a viscous fluid were developed for the grease and brash ice that can occupy the outskirts of the marginal ice zone [Weber, 1987, Keller, 1998]. One theory considers an asymptotically thin ice layer floating on a slightly viscous ocean (i.e., the water is no longer governed by potential-flow theory), where the viscosity in the ice layer is so large that it imposes a no-slip condition at the water surface, which creates a viscous boundary layer [Weber, 1987, Shen, 2022]. The resulting attenuation rate is such that

$$\alpha \propto \sqrt{\nu_{\mathrm{wtr}}}\, f^{5/2}, \tag{25}$$

where ν_{wtr} is the kinematic water viscosity [Weber, 1987]. For appropriately selected ν_{wtr}-values from 0.01–0.2 $\mathrm{m}^2\,\mathrm{s}^{-1}$, the theoretical predictions were shown to give reasonable agreement with observations by the Scott Polar Research Institute in the Arctic marginal ice zone, in far more general marginal ice zone conditions than the brash/grease ice the model was designed to represent [Weber, 1987]. An alternative viscous boundary layer theory for wave attenuation considers a thin elastic plate (possibly with compression), as a model of a marginal ice zone consisting of compacted ice floes, floating on viscous water [Liu and Mollo-Christensen, 1988]. The ice cover is assumed to impose a no-slip condition on the water surface, and the resulting attenuation rate is

$$\alpha \propto \frac{\kappa_0 \sqrt{\nu_{\mathrm{wtr}} f}}{c_{\mathrm{g}} (1 + \kappa_0 m)} \quad \text{where} \quad c_{\mathrm{g}} = 2\pi \frac{\mathrm{d} f}{\mathrm{d}\kappa_0} \quad \text{is the group velocity.} \tag{26}$$

The attenuation rate was found to give reasonable agreement with Arctic marginal ice zone observations for chosen ν_{wtr}-values that spanned a range of four orders of magnitude [Liu et al., 1991a].

Another theory for grease ice as a viscous fluid considers an ice layer to be of finite thickness and finite viscosity, floating on an inviscid ocean, so that wave attenuation occurs in the ice layer only [Keller, 1998]. It predicts an attenuation rate $\alpha \propto \nu_{\mathrm{ice}} f^5$ for long waves, where ν_{ice} is the kinematic viscosity of the ice layer. An elastic response of the ice layer was incorporated into the theory [Wang and Shen, 2010], such that it connects with the landfast ice models, although the nature of the elastic response of the ice cover for small floes in the marginal ice zone must be reinterpreted (in an unspecified manner). The finite thickness viscoelastic model supports multiple types of wave modes that can swap dominance as parameters are varied, which makes identifying the dominant mode challenging in general [Wang and Shen, 2010, Zhao et al., 2017]. However, for a wide parameter range, the dominant mode can be approximated by a thin plate model, which results in a dispersion relation of the form (13b) with a complex F, such that the imaginary component is proportional to frequency [Mosig et al., 2015]. The model was shown to give an attenuation rate within the uncertainty bounds of the observations during SIPEX II, although using an elastic modulus several orders of magnitude greater than measured in consolidated sea ice, which has the effect of making the wavelengths in the marginal ice zone much greater than in the open ocean. In contrast, the attenuation rate predicted by the model with damping proportional to the ice displacement velocity (19) gives comparable agreement with the SIPEX II observations, but using an elastic modulus a couple of orders of magnitude less than that of consolidated sea ice, so that wavelengths are similar to their open-water counterparts [Mosig et al., 2015].

The viscous fluid ice layer theory was extended to model a mixture of grease and pancake ice [De Santi and Olla, 2017], which is characteristic of the winter Antarctic marginal ice zone [Alberello et al., 2019] and regions of the contemporary Arctic marginal ice zone [Cheng et al., 2017]. The pancakes are modelled as small rigid disks that apply no-slip conditions at the surface of the viscous fluid relative to their motion, and, thus, modify the stress at the surface of the ice layer [De Santi and Olla, 2017]. In conditions where the pancakes are close enough to collide, the theory is adapted to treat interacting pancakes as being locked together during the compression phase of the interaction. The resulting "close-packing" theory gives an attenuation rate [De Santi and Olla, 2017, Shen, 2022]

$$\alpha \propto \frac{f^5}{\nu_{\mathrm{ice}}}, \tag{27}$$

where the appearance of the viscosity parameter on the denominator contrasts with its appearance on the numerator in the theory without pancakes [Keller, 1998]. The ice-layer thickness and viscosity were estimated for the theories with and without pancakes by comparing to attenuation rate observations in grease–pancake conditions, and it was found that the viscosity parameter for the best-fits varied less for the theory with pancakes [De Santi et al., 2018].

Wave attenuation theories that go beyond the exponential attenuation paradigm have been proposed [Wadhams, 1973, Shen and Squire, 1998, Kohout et al., 2011, Squire, 2018]. The theories proposed cover distinct mechanisms for attenuation, but they share a governing equation for the wave amplitude, $A(x)$, of the form

$$\frac{\mathrm{d}A}{\mathrm{d}x} = -\tilde{\alpha}\, A^n, \tag{28}$$

which gives exponential attenuation only in the case that $n = 1$. This class of model includes one of the earliest wave attenuation theories [Wadhams, 1973], in which attenuation results from creep (inelastic bending) of the sea ice cover in response to waves, with the ice cover modelled as the standard floating elastic plate. An exponent $n = 3$ was chosen based on its use for ice shelves and it giving reasonable agreement with wave attenuation observations available at that time [Wadhams, 1973]. The creep theory for wave attenuation has been rediscovered and adapted with an ad-hoc factor that reduces the attenuation when wavelengths become much greater than floe sizes [Boutin et al., 2018], to give a model that somewhat replicates the change in wave attenuation inferred from observations before and after ice breakup events [Boutin et al., 2018, Ardhuin et al., 2020].

3.3 Waves in ice shelves

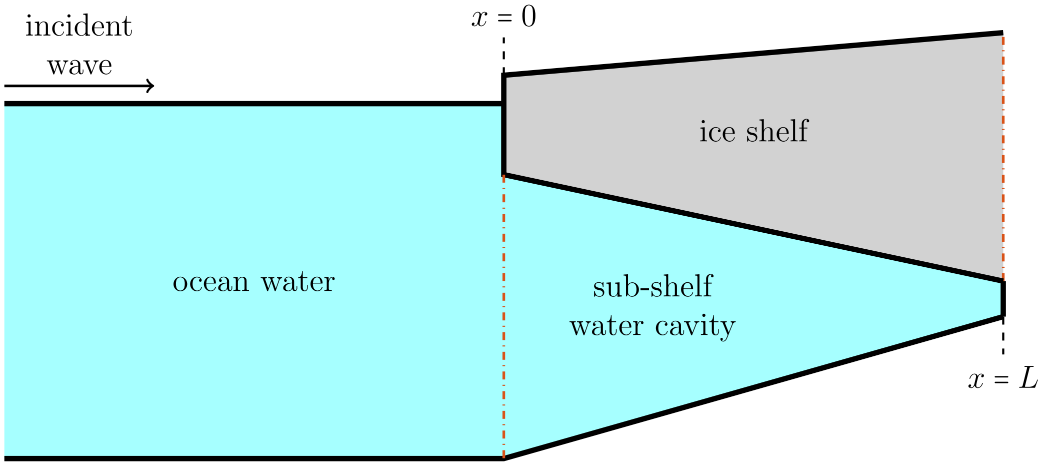

Figure 3: Schematic (not to scale) of the equilibrium geometry for a theoretical model of ocean wave propagation into and through an ice shelf.

The standard theoretical model for ocean waves propagating into and through landfast ice (§ 3.1; Fig. 1) has been used directly for ice shelves, although with representative geometrical parameters, i.e., thicker ice and shallower water [Fox and Squire, 1991]. Results from the standard Kirchoff thin-plate model for floating ice were compared with results from Timoshenko–Mindlin "thick-plate models", finding that the additional terms in the thick-plate model, such as rotational inertia, have negligible influence in the relevant parameter ranges [Fox and Squire, 1991, Balmforth and Craster, 1999]. Thus, there has been little subsequent interest in using thick-plate models. The model has been extended to include the change in water depth between the open ocean and sub-shelf water cavity due to the Archimedean draught of the ice shelf, and it was used to show the draught has a major influence on model predictions over relevant wave periods, ranging from swell to tsunamis [Kalyanaraman et al., 2019].

Another common approach is to restrict calculations to a finite interval occupied by the ice shelf and sub-shelf water cavity ($x \in [0, L]$ in Fig. 3). Clamped conditions (zero displacement and slope of the ice shelf displacement) are usually applied at the grounding line, $x = L$, assuming that they represent the transition to the ice shelf becoming a grounded ice sheet for $x > L$, although hinged conditions have also been proposed [Holdsworth and Glynn, 1981]. The system is closed by prescribing (artificial) conditions along the water column beneath the ice shelf, where no water pressure [Holdsworth and Glynn, 1978, 1981] and no flux (zero horizontal water velocity) [Sergienko, 2013, Meylan et al., 2017] have both been used. Thus, the problem is unforced, and non-trivial solutions are normal modes that exist at a discrete set of wave periods and are only defined up to an unknown amplitude.

The normal modes represent near-resonant responses of the problem in which the shelf/cavity region is connected to the open ocean, and is forced by incident waves (Fig. 3) [Papathanasiou et al., 2019]. The connection allows resonant energy in the shelf/cavity region to leak into the open ocean, such that the normal modes for the decoupled problem become "complex resonances", where the associated wave periods have imaginary components and large (but finite) responses occur for nearby real-valued wave periods [Bennetts and Meylan, 2021]. Depending on the parameters, particularly the wave period, the complex resonances can be better approximated by either the no-pressure or no-flux conditions [Bennetts and Meylan, 2021]. The problem can also be viewed as a modification of the landfast-ice-type model to have a finite length shelf/cavity region [Vinogradov and Holdsworth, 1985, Kalyanaraman et al., 2019]. Those that approach the problem from the normal mode perspective usually assume shallow-water theory, based on wavelengths in the shelf/cavity region being much greater than the cavity depth [Vinogradov and Holdsworth, 1985, Papathanasiou et al., 2019], whereas those who approach the problem as a modified version of the landfast ice problem tend to use potential-flow theory (finite depth water) [Ilyas et al., 2018, Meylan et al., 2021, Bennetts and Meylan, 2021]. When the shelf/cavity region is connected to the open ocean, shallow-water theory is often inaccurate in the swell regime, as the open-ocean wavelengths are not necessarily long in relation to the water depth [Kalyanaraman et al., 2019]. In contrast, the "single-mode approximation" is accurate for the range of relevant wave periods, and has a similarly simple structure to the shallow-water approximation [Bennetts and Meylan, 2021, Liang et al., 2024].

The earliest theoretical models identified the potential importance of spatial variations in the geometry (ice shelf thickness and underlying seabed) and three-dimensional effects [Holdsworth and Glynn, 1978, 1981]. However, both demand numerical solution methods, and were largely overlooked until more efficient computational approaches were developed. Idealised spatial variations in two-dimensional geometries have been investigated, including the effects of the ice shelf thickening and the seabed shoaling away from the shelf front (Fig. 3) [Meylan et al., 2021, Bennetts and Meylan, 2021], and blocking of waves over certain wave-period bands (i.e., stop-gaps) by periodic distributions of crevasses or surface rolls [Freed-Brown et al., 2012, Nekrasov and MacAyeal, 2023]. Geometries along transects through specific ice shelves have been incorported into models [Kalyanaraman et al., 2021, Bennetts et al., 2022c, Liang et al., 2024], and have been used to show that ice shelf flexure in response to swell is amplified by up to an order of magnitude at regions of local thinning (e.g., crevasses), whereas infragravity waves and very long period waves are amplified at regions of local cavity depth thinning [Bennetts et al., 2022c, Liang et al., 2024]. Analysis for three-dimensional models has been more restricted, but has included numerical computation of normal modes for circular, semi-circular and square ice shelves [Papathanasiou and Belibassakis, 2019], and time-domain simulations for models of specific ice shelves [Sergienko, 2017, Tazhimbetov et al., 2023].

Theoretical models have also been investigated in which the ice shelf is treated as an elastic body of finite thickness, i.e., they do not assume the ice shelf is a plate [Sergienko, 2010, 2017, Kalyanaraman et al., 2020, 2021, Abrahams et al., 2023, Bennetts et al., 2024a]. Initial studies invoked other assumptions, such as no inertia (assuming very long waves) [Sergienko, 2010, 2017], or zero gravitational forcing [Kalyanaraman et al., 2020, 2021]. A numerical solution method was used to conduct time-domain simulations with the full linear equations of elasticity in two dimensions and including gravitational forcing, and showed extensional Lamb waves are excited in addition to flexural-gravity waves [Abrahams et al., 2023]. Subsequently, a thin-plate theory was derived in which extensional Lamb waves are generated by coupling between the water and ice shelf at the shelf front [Bennetts et al., 2024a]. The new theory was used to show that extensional waves significantly increase ice shelf flexure in the swell regime in comparison to a theory with flexural-gravity waves alone [Bennetts et al., 2024a].

4 Perspectives and outlooks

Research to understand waves in the marginal ice zone is currently a major international and interdisciplinary research effort. The focus on wave attenuation has persisted throughout the evolution of the research field since it first came to prominence in the 1970s. There are now far more observations of wave attenuation, but the central question of what mechanisms govern attenuation in the marginal ice zone remains elusive. The observations have served the important purpose of illustrating the challenging physics of wave attenuation in the marginal ice zone. The associated question of how the attenuation rate depends on the ice cover properties also remains largely unresolved. This is arguably a lower hanging fruit, as it seems likely that building on the currently limited observations of wave attenuation and accompanying ice properties [Alberello et al., 2022] will reveal key relationships. It may then be possible to limit the viable theories for wave attenuation, in a similar way to how observed power-law relationships between the attenuation rate, α, and wave period have been used [Meylan et al., 2018].

Growth of the research fields on waves in landfast ice and ice shelves could follow that of waves in the marginal ice zone in the near future. There is already evidence of the growth for waves in ice shelves, motivated by the increased loss of ice shelf mass to calving [Greene et al., 2022], and thinning [Paolo et al., 2015], which leaves the ice shelves more susceptible to damaging wave-induced flexure [Bassis et al., 2024]. There is also increased recognition that landfast ice has important impacts on the Earth system, despite only occupying a small fraction of the overall sea ice cover [Fraser et al., 2023]. Thus, landfast ice breakup due to ocean waves is likely to play a major role in future studies, in a similar way that wave-induced breakup of large floes has played a leading role in studies of marginal ice zone dynamics over the past decade [Bennetts et al., 2022a, Dumont, 2022]. Moreover, the three waves-in-ice sub-fields are becoming increasingly interconnected. Large amplitude ocean swell are more likely to reach ice shelves now that the protective pack ice barrier is retreating [Teder et al., 2022], and there is evidence that prolonged periods of flexure forced by swell triggered catastrophic calving events [Massom et al., 2018, Teder et al., 2025]. Moreover, landfast ice connected to a shelf front provides an additional protective barrier from swell [Teder et al., 2025], as well as stabilising back-stress for the ice shelf [Greene et al., 2018]. Therefore, there is a need to move towards research on waves in the coupled marginal ice zone–landfast ice–ice shelf system.

Acknowledgements

LGB is funded by the Australian Research Council (FT190100404, DP240100325).

References

Luke G Bennetts, Timothy D Williams, and Richard Porter. A thin-plate approximation for ocean wave interactions with an ice shelf. *Journal of Fluid Mechanics*, 984:A48, 2024a.

Luke G Bennetts, Cecilia M Bitz, Daniel L Feltham, Alison L Kohout, and Michael H Meylan. Marginal ice zone dynamics: future research perspectives and pathways. *Philosophical Transactions of the Royal Society A*, 380(2235):20210267, 2022a.

Vernon A Squire. Past, present and impendent hydroelastic challenges in the polar and subpolar seas. *Philosophical Transactions of the Royal Society A*, 369(1947):2813–2831, 2011.

Alison L Kohout, Michael JM Williams, Sam M Dean, and Michael H Meylan. Storm-induced sea-ice breakup and the implications for ice extent. *Nature*, 509(7502):604–607, 2014.

Jim Thomson, Stephen Ackley, Fanny Girard-Ardhuin, Fabrice Ardhuin, Alex Babanin, Guillaume Boutin, John Brozena, Sukun Cheng, Clarence Collins, Martin Doble, et al. Overview of the Arctic sea state and boundary layer physics program. *Journal of Geophysical Research: Oceans*, 123(12):8674–8687, 2018.

Alison L Kohout, Madison Smith, Lettie A Roach, Guy Williams, Fabien Montiel, and Michael JM Williams. Observations of exponential wave attenuation in Antarctic sea ice during the PIPERS campaign. *Annals of Glaciology*, 61(82):196–209, 2020.

Luke G Bennetts, Cecilia M Bitz, Daniel L Feltham, Alison L Kohout, and Michael H Meylan. Theory, modelling and observations of marginal ice zone dynamics: multidisciplinary perspectives and outlooks, 2022b.

Vernon A Squire. Marginal ice zone dynamics. *Philosophical Transactions of the Royal Society A*, 380(2235):20210266, 2022a.

Vernon A Squire. A prognosticative synopsis of contemporary marginal ice zone research. *Philosophical Transactions of the Royal Society A*, 380(2235):20220094, 2022b.

Greg B Crocker and Peter Wadhams. Breakup of Antarctic fast ice. *Cold Regions Science and Technology*, 17(1):61–76, 1989.

Kelly M Brunt, Emile A Okal, and Douglas R MacAyeal. Antarctic ice-shelf calving triggered by the Honshu (Japan) earthquake and tsunami, March 2011. *Journal of Glaciology*, 57(205): 785–788, 2011.

Peter D Bromirski, Olga V Sergienko, and Douglas R MacAyeal. Transoceanic infragravity waves impacting Antarctic ice shelves. *Geophysical Research Letters*, 37(2), 2010.

Robert A Massom, Theodore A Scambos, Luke G Bennetts, Phillip Reid, Vernon A Squire, and Sharon E Stammerjohn. Antarctic ice shelf disintegration triggered by sea ice loss and ocean swell. *Nature*, 558(7710):383–389, 2018.

Aiguo Zhao, Yuan Cheng, Alexander D Fraser, Luke G Bennetts, Haifeng Xiao, Qi Liang, Teng Li, and Rongxing Li. Long-term evolution of the Sulzberger Ice Shelf, West Antarctica: Insights from 74-year observations and 2022 Hunga-Tonga volcanic tsunami-induced calving. *Earth and Planetary Science Letters*, 646:118958, 2024.

Vernon A Squire, John P Dugan, Peter Wadhams, Philip J Rottier, and Antony K Liu. Of ocean waves and sea ice. *Annual Review of Fluid Mechanics*, 27(1):115–168, 1995.

Vernon A Squire. Of ocean waves and sea-ice revisited. *Cold Regions Science and Technology*, 49(2):110–133, 2007.

Vernon A Squire. Ocean wave interactions with sea ice: A reappraisal. *Annual Review of Fluid Mechanics*, 52:37–60, 2020.

Hayley H Shen. Modelling ocean waves in ice-covered seas. *Applied Ocean Research*, 83:30–36, 2019.

Takuji Waseda, Alberto Alberello, Takehiko Nose, Takenobu Toyota, Tsubasa Kodaira, and Yasushi Fujiwara. Observation of anomalous spectral downshifting of waves in the Okhotsk Sea marginal ice zone. *Philosophical Transactions of the Royal Society A*, 380(2235):20210256, 2022.

Alessandro Toffoli, Jordan PA Pitt, Alberto Alberello, and Luke G Bennetts. Modelling attenuation of irregular wave fields by artificial ice floes in the laboratory. *Philosophical Transactions of the Royal Society A*, 380(2235):20210255, 2022.

Will Perrie, Michael H Meylan, Bechara Toulany, and Michael P Casey. Modelling wave–ice interactions in three dimensions in the marginal ice zone. *Philosophical Transactions of the Royal Society A*, 380(2235):20210263, 2022.

Hayley H Shen. Wave-in-ice: theoretical bases and field observations. *Philosophical Transactions of the Royal Society A*, 380(2235):20210254, 2022.

Jim Thomson. Wave propagation in the marginal ice zone: connections and feedback mechanisms within the air–ice–ocean system. *Philosophical Transactions of the Royal Society A*, 380(2235):20210251, 2022.

Kenneth M Golden, Luke G Bennetts, Elena Cherkaev, Ian Eisenman, Daniel Feltham, Christopher Horvat, Elizabeth Hunke, Christopher Jones, Donald K Perovich, Pedro Ponte-Castaneda, et al. Modeling sea ice. *Notices of the American Mathematical Society*, 67(10): 1535–1555, 2020.

Luke G Bennetts, Callum J Shakespeare, Catherine A Vreugdenhil, Annie Foppert, Bishakhdatta Gayen, Amelie Meyer, Adele K Morrison, Laurie Padman, Helen E Phillips, Craig L Stevens, et al. Closing the loops on Southern Ocean dynamics: From the circumpolar current to ice shelves and from bottom mixing to surface waves. *Reviews of Geophysics*, 62 (3):e2022RG000781, 2024b.

Alex D Fraser, Pat Wongpan, Patricia J Langhorne, AR Klekociuk, K Kusahara, D Lannuzel, Robert A Massom, Klaus M Meiners, KM Swadling, Daniel P Atwater, et al. Antarctic landfast sea ice: A review of its physics, biogeochemistry and ecology. *Reviews of Geophysics*, 61(2):e2022RG000770, 2023.

Vernon A Squire and Alastair Allan. *Propagation of flexural gravity waves in sea ice*. Centre for Cold Ocean Resources Engineering, Memorial University of Newfoundland, 1977.

Vernon A Squire. A theoretical, laboratory, and field study of ice-coupled waves. *Journal of Geophysical Research: Oceans*, 89(C5):8069–8079, 1984a.

Graig Sutherland and Jean Rabault. Observations of wave dispersion and attenuation in landfast ice. *Journal of Geophysical Research: Oceans*, 121(3):1984–1997, 2016.

Joey J Voermans, Qingxiang Liu, Aleksey Marchenko, Jean Rabault, Kirill Filchuk, Ivan Ryzhov, Petra Heil, Takuji Waseda, Takehiko Nose, Tsubasa Kodaira, et al. Wave dispersion and dissipation in landfast ice: comparison of observations against models. *The Cryosphere*, 15(12):5557–5575, 2021.

Gordon de Q Robin. Wave propagation through fields of pack ice. *Philosophical Transactions of the Royal Society A*, 255(1057):313–339, 1963.

Peter Wadhams. Airborne laser profiling of swell in an open ice field. *Journal of Geophysical Research*, 80(33):4520–4528, 1975.

Peter Wadhams. Wave decay in the marginal ice zone measured from a submarine. *Deep Sea Research*, 25(1):23–40, 1978.

Vernon A Squire and Stuart C Moore. Direct measurement of the attenuation of ocean waves by pack ice. *Nature*, 283(5745):365–368, 1980.

Peter Wadhams. The marginal ice zone experiment (MIZEX) 1984: Scott Polar Research Institute participation. *Polar record*, 22(140):505–510, 1985.

Peter Wadhams, Vernon A Squire, JA Ewing, and RW Pascal. The effect of the marginal ice zone on the directional wave spectrum of the ocean. *Journal of physical oceanography*, 16(2): 358–376, 1986.

Peter Wadhams, Vernon A Squire, Dougal J Goodman, Andrew M Cowan, and Stuart C Moore. The attenuation rates of ocean waves in the marginal ice zone. *Journal of Geophysical Research: Oceans*, 93(C6):6799–6818, 1988.

Peter Wadhams and Benjamin Holt. Waves in frazil and pancake ice and their detection in Seasat synthetic aperture radar imagery. *Journal of Geophysical Research: Oceans*, 96(C5): 8835–8852, 1991.

Antony K Liu, Benjamin Holt, and Paris W Vachon. Wave propagation in the marginal ice zone: Model predictions and comparisons with buoy and synthetic aperture radar data. *Journal of Geophysical Research: Oceans*, 96(C3):4605–4621, 1991a.

Antony K Liu, Paris W Vachon, and Chih Y Peng. Observation of wave refraction at an ice edge by synthetic aperture radar. *Journal of Geophysical Research: Oceans*, 96(C3):4803–4808, 1991b.

Pierre Larouche and Claude Cariou. Directional wave spectra estimation in a marginal ice zone using linear prediction. *Journal of Physical Oceanography*, 22(2):196–206, 1992.

Peter Wadhams, F Parmiggiani, and G De Carolis. The use of SAR to measure ocean wave dispersion in frazil–pancake icefields. *Journal of Physical Oceanography*, 32(6):1721–1746, 2002.

Peter Wadhams, FF Parmiggiani, G De Carolis, D Desiderio, and Martin J Doble. Sar imaging of wave dispersion in Antarctic pancake ice and its use in measuring ice thickness. *Geophysical Research Letters*, 31(15), 2004.

Martin J Doble and Jean-Raymond Bidlot. Wave buoy measurements at the Antarctic sea ice edge compared with an enhanced ECMWF WAM: Progress towards global waves-in-ice modelling. *Ocean Modelling*, 70:166–173, 2013.

Martin J Doble, Giacomo De Carolis, Michael H Meylan, Jean-Raymond Bidlot, and Peter Wadhams. Relating wave attenuation to pancake ice thickness, using field measurements and model results. *Geophysical Research Letters*, 42(11):4473–4481, 2015.

Michael H Meylan, Luke G Bennetts, and Alison L Kohout. In situ measurements and analysis of ocean waves in the Antarctic marginal ice zone. *Geophysical Research Letters*, 41(14): 5046–5051, 2014.

Sukun Cheng, W Erick Rogers, Jim Thomson, Madison Smith, Martin J Doble, Peter Wadhams, Alison L Kohout, Björn Lund, Ola PG Persson, Clarence O Collins III, et al. Calibrating a viscoelastic sea ice model for wave propagation in the Arctic fall marginal ice zone. *Journal of Geophysical Research: Oceans*, 122(11):8770–8793, 2017.

Clarence Collins, Martin Doble, Björn Lund, and Madison Smith. Observations of surface wave dispersion in the marginal ice zone. *Journal of Geophysical Research: Oceans*, 123(5): 3336–3354, 2018.

F Montiel, VA Squire, M Doble, J Thomson, and P Wadhams. Attenuation and directional spreading of ocean waves during a storm event in the autumn Beaufort Sea marginal ice zone. *Journal of Geophysical Research: Oceans*, 123(8):5912–5932, 2018.

W Erick Rogers, Michael H Meylan, and Alison L Kohout. Estimates of spectral wave attenuation in Antarctic sea ice, using model/data inversion. *Cold Regions Science and Technology*, 182:103198, 2021.

Fabien Montiel, Alison L Kohout, and Lettie A Roach. Physical drivers of ocean wave attenuation in the marginal ice zone. *Journal of Physical Oceanography*, 52(5):889–906, 2022.

Marcello Vichi, Clare Eayrs, Alberto Alberello, Anriëtte Bekker, Luke G Bennetts, David Holland, Ehlke de Jong, Warren Joubert, Keith MacHutchon, Gabriele Messori, et al. Effects of an explosive polar cyclone crossing the Antarctic marginal ice zone. *Geophysical Research Letters*, 46(11):5948–5958, 2019.

Alberto Alberello, Luke G Bennetts, Petra Heil, Clare Eayrs, Marcello Vichi, Keith MacHutchon, Miguel Onorato, and Alessandro Toffoli. Drift of pancake ice floes in the winter Antarctic marginal ice zone during polar cyclones. *Journal of Geophysical Research: Oceans*, 125(3):e2019JC015418, 2020.

Takehiko Nose, Tomotaka Katsuno, Takuji Waseda, Shuki Ushio, Jean Rabault, Tsubasa Kodaira, and Joey Voermans. Observation of wave propagation over 1,000 km into Antarctica winter pack ice. *Coastal Engineering Journal*, 66(1):115–131, 2024.

Fabrice Ardhuin, Mark Otero, Sophia Merrifield, Antoine Grouazel, and Eric Terrill. Ice breakup controls dissipation of wind waves across Southern Ocean sea ice. *Geophysical Research Letters*, 47(13):e2020GL087699, 2020.

Peter Sutherland and Jean-Claude Gascard. Airborne remote sensing of ocean wave directional wavenumber spectra in the marginal ice zone. *Geophysical Research Letters*, 43(10):5151–5159, 2016.

Peter Sutherland, John Brozena, W Erick Rogers, Martin Doble, and Peter Wadhams. Airborne remote sensing of wave propagation in the marginal ice zone. *Journal of Geophysical Research: Oceans*, 123(6):4132–4152, 2018.

Fabrice Ardhuin, Fabrice Collard, Bertrand Chapron, Fanny Girard-Ardhuin, Gilles Guitton, Alexis Mouche, and Justin E Stopa. Estimates of ocean wave heights and attenuation in sea ice using the SAR wave mode on Sentinel-1A. *Geophysical Research Letters*, 42(7):2317–2325, 2015.

Fabrice Ardhuin, Justin Stopa, Bertrand Chapron, Fabrice Collard, Madison Smith, Jim Thomson, Martin Doble, Byron Blomquist, Ola Persson, Clarence O Collins III, et al. Measuring ocean waves in sea ice using SAR imagery: A quasi-deterministic approach evaluated with Sentinel-1 and in situ data. *Remote sensing of Environment*, 189:211–222, 2017.

Justin E Stopa, Fabrice Ardhuin, Jim Thomson, Madison M Smith, Alison Kohout, Martin Doble, and Peter Wadhams. Wave attenuation through an Arctic marginal ice zone on 12 October 2015: 1. Measurement of wave spectra and ice features from Sentinel 1A. *Journal of Geophysical Research: Oceans*, 123(5):3619–3634, 2018a.

Justin E Stopa, Peter Sutherland, and Fabrice Ardhuin. Strong and highly variable push of ocean waves on Southern Ocean sea ice. *Proceedings of the National Academy of Sciences*, 115(23):5861–5865, 2018b.

Bing Qing Huang and Xiao-Ming Li. Wave attenuation by sea ice in the Arctic marginal ice zone observed by spaceborne sar. *Geophysical Research Letters*, 50(21):e2023GL105059, 2023.

Christopher Horvat, Ed Blanchard-Wrigglesworth, and Alex Petty. Observing waves in sea ice with ICESat-2. *Geophysical Research Letters*, 47(10):e2020GL087629, 2020.

Jill Brouwer, Alexander D Fraser, Damian J Murphy, Pat Wongpan, Alberto Alberello, Alison Kohout, Christopher Horvat, Simon Wotherspoon, Robert A Massom, Jessica Cartwright, et al. Altimetric observation of wave attenuation through the Antarctic marginal ice zone using ICESat-2. *The Cryosphere*, 16(6):2325–2353, 2022.

Momme C Hell and Christopher Horvat. A method for constructing directional surface wave spectra from ICESat-2 altimetry. *The Cryosphere*, 18(1):341–361, 2024.

Edward Thiel, AP Crary, Richard A Haubrich, and John C Behrendt. Gravimetric determination of ocean tide, Weddell and Ross Seas, Antarctica. *Journal of Geophysical Research*, 65 (2):629–636, 1960.

RT Williams and ES Robinson. Flexural waves in the Ross Ice Shelf. *Journal of Geophysical Research: Oceans*, 86(C7):6643–6648, 1981.

WH Robinson and TG Haskell. Travelling flexural waves in the Erebus Glacier Tongue, McMurdo Sound, Antarctica. *Cold Regions Science and Technology*, 20(3):289–293, 1992.

Vernon A Squire, William H Robinson, Michael Meylan, and Timothy G Haskell. Observations of flexural waves on the Erebus Ice Tongue, McMurdo Sound, Antarctica, and nearby sea ice. *Journal of Glaciology*, 40(135):377–385, 1994.

William H Robinson and Timothy G Haskell. Calving of Erebus Glacier Tongue. *Nature*, 346 (6285):615–616, 1990.

Douglas R MacAyeal, Emile A Okal, Richard C Aster, Jeremy N Bassis, Kelly M Brunt, L Mac Cathles, Robert Drucker, Helen A Fricker, Young-Jin Kim, Seelye Martin, et al. Transoceanic wave propagation links iceberg calving margins of Antarctica with storms in tropics and Northern Hemisphere. *Geophysical Research Letters*, 33(17), 2006.

LM Cathles IV, Emile A Okal, and Douglas R MacAyeal. Seismic observations of sea swell on the floating Ross Ice Shelf, Antarctica. *Journal of Geophysical Research: Earth Surface*, 114 (F2), 2009.

Peter D Bromirski and Ralph A Stephen. Response of the Ross Ice Shelf, Antarctica, to ocean gravity-wave forcing. *Annals of Glaciology*, 53(60):163–172, 2012.

Peter D Bromirski, A Diez, P Gerstoft, Ralph A Stephen, T Bolmer, DA Wiens, RC Aster, and A Nyblade. Ross Ice Shelf vibrations. *Geophysical Research Letters*, 42(18):7589–7597, 2015.

Peter D Bromirski, Zhao Chen, Ralph A Stephen, Peter Gerstoft, D Arcas, Anja Diez, Richard C Aster, Douglas A Wiens, and Andrew Nyblade. Tsunami and infragravity waves impacting Antarctic ice shelves. *Journal of Geophysical Research: Oceans*, 122(7):5786–5801, 2017.

Zhao Chen, Peter D Bromirski, Peter Gerstoft, Ralph A Stephen, Douglas A Wiens, Richard C Aster, and Andrew A Nyblade. Ocean-excited plate waves in the Ross and Pine Island Glacier ice shelves. *Journal of Glaciology*, 64(247):730–744, 2018.

Zhao Chen, Peter D Bromirski, Peter Gerstoft, Ralph A Stephen, Won Sang Lee, Sukyoung Yun, Stephanie D Olinger, Richard C Aster, Douglas A Wiens, and Andrew A Nyblade. Ross Ice Shelf icequakes associated with ocean gravity wave activity. *Geophysical Research Letters*, 46(15):8893–8902, 2019.

Colin Fox and Vernon A Squire. Reflection and transmission characteristics at the edge of shore fast sea ice. *Journal of Geophysical Research: Oceans*, 95(C7):11629–11639, 1990.

Colin Fox and Vernon A Squire. On the oblique reflexion and transmission of ocean waves at shore fast sea ice. *Philosophical Transactions of the Royal Society A*, 347(1682):185–218, 1994.

Hyuck Chung and Colin Fox. Calculation of wave propagation into land-fast ice. *Annals of Glaciology*, 33:322–326, 2001.

Christopher M Linton and Philip McIver. *Handbook of mathematical techniques for wave/structure interactions*. Chapman and Hall/CRC, 2001.

Timothy D Williams. *Reflections on ice: Scattering of flexural Gravity waves by irregularities in Arctic and Antarctic ice sheets*. PhD thesis, University of Otago, 2006.

Luke G Bennetts. *Wave scattering by ice sheets of varying thickness*. PhD thesis, University of Reading, 2007.

Vernon A Squire. On the critical angle for ocean waves entering shore fast ice. *Cold Regions Science and Technology*, 10(1):59–68, 1984b.

NJ Robinson and SC Palmer. A modal analysis of a rectangular plate floating on an incompressible liquid. *Journal of Sound and Vibration*, 142(3):453–460, 1990.

Vernon A Squire and Colin Fox. On ice coupled waves: a comparison of data and theory. In *Advances in ice technology: Proc. 3rd Int. Conf. on Ice Technology*, pages 269–280. Computational Mechanics Publications Cambridge, MA, 1992.

Vernon A Squire. The breakup of shore fast sea ice. *Cold Regions Science and Technology*, 21 (3):211–218, 1993.

Michael H Meylan and Vernon A Squire. The response of ice floes to ocean waves. *Journal of Geophysical Research: Oceans*, 99(C1):891–900, 1994.

Luke G Bennetts and Vernon A Squire. On the calculation of an attenuation coefficient for transects of ice-covered ocean. *Proceedings of the Royal Society A*, 468(2137):136–162, 2012a.

Alison L Kohout and Michael H Meylan. An elastic plate model for wave attenuation and ice floe breaking in the marginal ice zone. *Journal of Geophysical Research: Oceans*, 113(C9), 2008.

Luke G Bennetts and Vernon A Squire. Model sensitivity analysis of scattering-induced attenuation of ice-coupled waves. *Ocean Modelling*, 45:1–13, 2012b.

Luke G Bennetts and Vernon A Squire. Wave scattering by multiple rows of circular ice floes. *Journal of Fluid Mechanics*, 639:213–238, 2009.

Malte A Peter and Michael H Meylan. Water-wave scattering by vast fields of bodies. *SIAM Journal on Applied Mathematics*, 70(5):1567–1586, 2010.

Luke G Bennetts, Malte A Peter, Vernon A Squire, and Michael H Meylan. A three-dimensional model of wave attenuation in the marginal ice zone. *Journal of Geophysical Research: Oceans*, 115(C12), 2010.

Fabien Montiel, Vernon A Squire, and Luke G Bennetts. Attenuation and directional spreading of ocean wave spectra in the marginal ice zone. *Journal of Fluid Mechanics*, 790:492–522, 2016.

Malte A Peter, Michael H Meylan, and Hyuck Chung. Wave scattering by a circular elastic plate in water of finite depth: a closed form solution. *International Journal of Offshore and Polar Engineering*, 14(02), 2004.

Michael H Meylan. Wave response of an ice floe of arbitrary geometry. *Journal of Geophysical Research: Oceans*, 107(C1):5–1, 2002.

Luke G Bennetts and Timothy D Williams. Wave scattering by ice floes and polynyas of arbitrary shape. *Journal of Fluid Mechanics*, 662:5–35, 2010.

Luke G Bennetts and Vernon A Squire. Linear wave forcing of an array of axisymmetric ice floes. *IMA Journal of Applied Mathematics*, 75(1):108–138, 2010.

Vernon A Squire and Fabien Montiel. Evolution of directional wave spectra in the marginal ice zone: a new model tested with legacy data. *Journal of Physical Oceanography*, 46(10): 3121–3137, 2016.

Diane Masson and PH LeBlond. Spectral evolution of wind-generated surface gravity waves in a dispersed ice field. *Journal of Fluid Mechanics*, 202:43–81, 1989.

Michael H Meylan, Vernon A Squire, and Colin Fox. Toward realism in modeling ocean wave behavior in marginal ice zones. *Journal of Geophysical Research: Oceans*, 102(C10):22981–22991, 1997.

Michael H Meylan and Diane Masson. A linear Boltzmann equation to model wave scattering in the marginal ice zone. *Ocean Modelling*, 11(3-4):417–427, 2006.

Michael H Meylan and Luke G Bennetts. Three-dimensional time-domain scattering of waves in the marginal ice zone. *Philosophical Transactions of the Royal Society A*, 376(2129): 20170334, 2018.

Luke G Bennetts and Timothy D Williams. Water wave transmission by an array of floating discs. *Proceedings of the Royal Society A*, 471(2173):20140698, 2015.

Xin Zhao and Hayley H Shen. A diffusion approximation for ocean wave scatterings by randomly distributed ice floes. *Ocean Modelling*, 107:21–27, 2016.

Jordan PA Pitt and Luke G Bennetts. On transitions in water wave propagation through consolidated to broken sea ice covers. *Proceedings of the Royal Society A*, 48020230862, 2024.

Azam Dolatshah, Filippo Nelli, Luke G Bennetts, Alberto Alberello, Michael H Meylan, Jason P Monty, and Alessandro Toffoli. Hydroelastic interactions between water waves and floating freshwater ice. *Physics of Fluids*, 30(9), 2018.

Giulio Passerotti, Luke G Bennetts, Franz von Bock und Polach, Alberto Alberello, Otto Puolakka, Azam Dolatshah, Jaak Monbaliu, and Alessandro Toffoli. Interactions between irregular wave fields and sea ice: A physical model for wave attenuation and ice breakup in an ice tank. *Journal of Physical Oceanography*, 52(7):1431–1446, 2022.

Michael H Meylan, Luke G Bennetts, JEM Mosig, WE Rogers, MJ Doble, and Malte A Peter. Dispersion relations, power laws, and energy loss for waves in the marginal ice zone. *Journal of Geophysical Research: Oceans*, 123(5):3322–3335, 2018.

Jan Erik Weber. Wave attenuation and wave drift in the marginal ice zone. *Journal of Physical Oceanography*, 17(12):2351–2361, 1987.

Joseph B Keller. Gravity waves on ice-covered water. *Journal of Geophysical Research: Oceans*, 103(C4):7663–7669, 1998.

Antony K Liu and Erik Mollo-Christensen. Wave propagation in a solid ice pack. *Journal of Physical Oceanography*, 18(11):1702–1712, 1988.

Ruixue Wang and Hayley H Shen. Gravity waves propagating into an ice-covered ocean: A viscoelastic model. *Journal of Geophysical Research: Oceans*, 115(C6), 2010.

Xin Zhao, Sukun Cheng, and Hayley H Shen. Nature of wave modes in a coupled viscoelastic layer over water. *Journal of Engineering Mechanics*, 143(10):04017114, 2017.

Johannes EM Mosig, Fabien Montiel, and Vernon A Squire. Comparison of viscoelastic-type models for ocean wave attenuation in ice-covered seas. *Journal of Geophysical Research: Oceans*, 120(9):6072–6090, 2015.

Francesca De Santi and Piero Olla. Effect of small floating disks on the propagation of gravity waves. *Fluid Dynamics Research*, 49(2):025512, 2017.

Alberto Alberello, Miguel Onorato, Luke Bennetts, Marcello Vichi, Clare Eayrs, Keith MacHutchon, and Alessandro Toffoli. Pancake ice floe size distribution during the winter expansion of the Antarctic marginal ice zone. *The Cryosphere*, 13(1):41–48, 2019.

Francesca De Santi, Giacomo De Carolis, Piero Olla, Martin Doble, Sukun Cheng, Hayley H Shen, Peter Wadhams, and Jim Thomson. On the ocean wave attenuation rate in grease-pancake ice, a comparison of viscous layer propagation models with field data. *Journal of Geophysical Research: Oceans*, 123(8):5933–5948, 2018.

Peter Wadhams. Attenuation of swell by sea ice. *Journal of Geophysical Research*, 78(18): 3552–3563, 1973.

Hayley H Shen and Vernon A Squire. Wave damping in compact pancake ice fields due to interactions between pancakes. *Antarctic Sea Ice: Physical Processes, Interactions and Variability*, 74:325–341, 1998.

Alison L Kohout, Michael H Meylan, and David R Plew. Wave attenuation in a marginal ice zone due to the bottom roughness of ice floes. *Annals of Glaciology*, 52(57):118–122, 2011.

Vernon A Squire. A fresh look at how ocean waves and sea ice interact. *Philosophical Transactions of the Royal Society A*, 376(2129):20170342, 2018.

Guillaume Boutin, Fabrice Ardhuin, Dany Dumont, Caroline Sévigny, Fanny Girard-Ardhuin, and Mickael Accensi. Floe size effect on wave-ice interactions: Possible effects, implementation in wave model, and evaluation. *Journal of Geophysical Research: Oceans*, 123(7): 4779–4805, 2018.

Colin Fox and Vernon A Squire. Coupling between the ocean and an ice shelf. *Annals of Glaciology*, 15:101–108, 1991.

Neil J Balmforth and Richard V Craster. Ocean waves and ice sheets. *Journal of Fluid Mechanics*, 395:89–124, 1999.

Balaje Kalyanaraman, Luke G Bennetts, Bishnu Lamichhane, and Michael H Meylan. On the shallow-water limit for modelling ocean-wave induced ice-shelf vibrations. *Wave Motion*, 90: 1–16, 2019.

Gerald Holdsworth and JE Glynn. A mechanism for the formation of large icebergs. *Journal of Geophysical Research: Oceans*, 86(C4):3210–3222, 1981.

Gerald Holdsworth and JE Glynn. Iceberg calving from floating glaciers by a vibrating mechanism. *Nature*, 274(5670):464–466, 1978.

Olga V Sergienko. Normal modes of a coupled ice-shelf/sub-ice-shelf cavity system. *Journal of Glaciology*, 59(213):76–80, 2013.

Michael H Meylan, Luke G Bennetts, Roger J Hosking, and Elliot Catt. On the calculation of normal modes of a coupled ice-shelf/sub-ice-shelf cavity system. *Journal of Glaciology*, 63 (240):751–754, 2017.

Theodosios K Papathanasiou, Angeliki E Karperaki, and Kostas A Belibassakis. On the resonant hydroelastic behaviour of ice shelves. *Ocean Modelling*, 133:11–26, 2019.

Luke G Bennetts and Michael H Meylan. Complex resonant ice shelf vibrations. *SIAM Journal on Applied Mathematics*, 81(4):1483–1502, 2021.

OG Vinogradov and Gerald Holdsworth. Oscillation of a floating glacier tongue. *Cold Regions Science and Technology*, 10(3):263–271, 1985.

Muhammad Ilyas, Michael H Meylan, Bishnu Lamichhane, and Luke G Bennetts. Time-domain and modal response of ice shelves to wave forcing using the finite element method. *Journal of Fluids and Structures*, 80:113–131, 2018.

Michael H Meylan, Muhammad Ilyas, Bishnu P Lamichhane, and Luke G Bennetts. Swell-induced flexural vibrations of a thickening ice shelf over a shoaling seabed. *Proceedings of the Royal Society A*, 477(2254):20210173, 2021.

Jie Liang, Jordan PA Pitt, and Luke G Bennetts. Pan-Antarctic assessment of ice shelf flexural responses to ocean waves. *Journal of Geophysical Research: Oceans*, 129(8):e2023JC020824, 2024.

Julian Freed-Brown, Jason M Amundson, Douglas R MacAyeal, and Wendy W Zhang. Blocking a wave: frequency band gaps in ice shelves with periodic crevasses. *Annals of glaciology*, 53 (60):85–89, 2012.

Peter Nekrasov and Douglas R MacAyeal. Ocean wave blocking by periodic surface rolls fortifies Arctic ice shelves. *Journal of Glaciology*, pages 1–11, 2023.

Balaje Kalyanaraman, Michael H Meylan, Bishnu P Lamichhane, and Luke G Bennetts. iceFEM: A freefem package for wave induced ice-shelf vibrations. *Journal of Open Source Software*, 6(59):2939, 2021.

Luke G Bennetts, Jie Liang, and Jordan PA Pitt. Modeling ocean wave transfer to Ross Ice Shelf flexure. *Geophysical Research Letters*, 49(21):e2022GL100868, 2022c.

Theodosios K Papathanasiou and Kostas A Belibassakis. A nonconforming hydroelastic triangle for ice shelf modal analysis. *Journal of Fluids and Structures*, 91:102741, 2019.

Olga V Sergienko. Behavior of flexural gravity waves on ice shelves: Application to the Ross Ice Shelf. *Journal of Geophysical Research: Oceans*, 122(8):6147–6164, 2017.

Nurbek Tazhimbetov, Martin Almquist, Jonatan Werpers, and Eric M Dunham. Simulation of flexural-gravity wave propagation for elastic plates in shallow water using an energy-stable finite difference method with weakly enforced boundary and interface conditions. *Journal of Computational Physics*, 493:112470, 2023.

Olga V Sergienko. Elastic response of floating glacier ice to impact of long-period ocean waves. *Journal of Geophysical Research: Earth Surface*, 115(F4), 2010.

Balaje Kalyanaraman, Michael H Meylan, Luke G Bennetts, and Bishnu P Lamichhane. A coupled fluid-elasticity model for the wave forcing of an ice-shelf. *Journal of Fluids and Structures*, 97:103074, 2020.

Lauren Abrahams, Jose Mierzejewski, Eric Dunham, and Peter D Bromirski. Ocean surface gravity wave excitation of flexural gravity and extensional Lamb waves in ice shelves. *Seismica*, 2(1), 2023.

Alberto Alberello, Luke G Bennetts, Miguel Onorato, Marcello Vichi, Keith MacHutchon, Clare Eayrs, Butteur Ntamba Ntamba, Alvise Benetazzo, Filippo Bergamasco, Filippo Nelli, et al. Three-dimensional imaging of waves and floes in the marginal ice zone during a cyclone. *Nature communications*, 13(1):4590, 2022.

Chad A Greene, Alex S Gardner, Nicole-Jeanne Schlegel, and Alexander D Fraser. Antarctic calving loss rivals ice-shelf thinning. *Nature*, 609(7929):948–953, 2022.

Fernando S Paolo, Helen A Fricker, and Laurie Padman. Volume loss from Antarctic ice shelves is accelerating. *Science*, 348(6232):327–331, 2015.

Jeremy N Bassis, Anna Crawford, Samuel B Kachuck, Douglas I Benn, Catherine Walker, Joanna Millstein, Ravindra Duddu, Jan Åström, Helen Fricker, and Adrian Luckman. Stability of ice shelves and ice cliffs in a changing climate. *Annual Review of Earth and Planetary Sciences*, 52, 2024.

Dany Dumont. Marginal ice zone dynamics: history, definitions and research perspectives. *Philosophical Transactions of the Royal Society A*, 380(2235):20210253, 2022.

Nathan J Teder, Luke G Bennetts, Philip A Reid, and Robert A Massom. Sea ice-free corridors for large swell to reach Antarctic ice shelves. *Environmental Research Letters*, 17(4):045026, 2022.

Nathan J Teder, Luke G Bennetts, Philip A Reid, Robert A Massom, Jordan PA Pitt, Theodore A Scambos, and Alex D Fraser. Large-scale ice shelf calving events follow prolonged amplifications in flexure. *Nature Geosciences*, page Under review, 2025.

Chad A Greene, Duncan A Young, David E Gwyther, Benjamin K Galton-Fenzi, and Donald D Blankenship. Seasonal dynamics of Totten Ice Shelf controlled by sea ice buttressing. *The Cryosphere*, 12(9):2869–2882, 2018.